HHS Public Access

Author manuscript

Sci Signal. Author manuscript; available in PMC 2020 April 11.

Published in final edited form as:

Sci Signal. ; 12(568): . doi:10.1126/scisignal.aau9216.

Inflammation, necrosis, and the kinase RIP3 are key mediators of AAG-dependent alkylation-induced retinal degeneration

Mariacarmela Allocca[1,2], **Joshua J. Corrigan**[1,2], **Aprotim Mazumder**[1,2], **Kimberly R. Fake**[1,2], **Leona D. Samson**[1,2,3,4,*]

[1]Department of Biological Engineering, Massachusetts Institute of Technology, 77 Massachusetts Avenue, Cambridge, MA 02139, USA.

[2]Center for Environmental Health Sciences, Massachusetts Institute of Technology, 77 Massachusetts Avenue, Cambridge, MA 02139, USA.

[3]Department of Biology, Massachusetts Institute of Technology, 77 Massachusetts Avenue, Cambridge, MA 02139, USA.

[4]David H. Koch Institute for Integrative Cancer Research, Massachusetts Institute of Technology, 77 Massachusetts Avenue, Cambridge, MA 02139, USA.

Abstract

DNA-alkylating agents are commonly used to kill cancer cells, but the base excision repair (BER) pathway they trigger can produce toxic intermediates that damage healthy tissues as well, including retinal degeneration (RD). Apoptosis, a process of programmed cell death, is assumed to be the main mechanism of this alkylation-induced photoreceptor (PR) cell death in RD. Here, we studied the involvement of necroptosis (another process of cell death) and inflammation in alkylation-induced RD. Male mice exposed to a methylating agent exhibited a reduced number of PR cell rows, active gliosis, and cytokine induction and macrophage infiltration in the retina. Dying PRs exhibited a necrotic morphology, increased 8-hydroxyguanosine (a marker of oxidative damage), and overexpression of the necroptosis-associated genes *Rip1* and *Rip3*. The activity of PARP1, an enzyme that mediates BER, cell death and inflammation, was increased in PR cells and associated with the release of proinflammatory chemokine and inflammatory ligand HMGB1 from PR nuclei. Deficiency of the anti-inflammatory cytokine IL-10 resulted in more severe RD, whereas deficiency of RIP3 conferred partial protection. Female mice were partially protected from alkylation-induced RD, showing reduced markers of necroptosis and inflammation compared to those in males. PRs in mice lacking the BER-initiating DNA glycosylase AAG did not exhibit alkylation-induced necroptosis or inflammation. Our findings show that AAG-initiated BER at alkylated DNA bases induces sex-dependent RD primarily by triggering necroptosis and activating

*Corresponding author. lsamson@mit.edu.

Author contributions: Conception and design: M.A. and L.D.S. Investigation: M.A., J.J.C., A.M., and K.R.F. Analysis and interpretation of data: M.A. and J.J.C. Writing and editing: M.A., J.J.C., and L.D.S. Project administration: M.A. and L.D.S. Funding acquisition: L.D.S.

Competing interests: The authors declare that they have no competing interests.

Data and materials availability: *Rip3*$^{-/-}$ mice require a material transfer agreement from Genentech. All data needed to evaluate the conclusions in the paper are present in the paper and/or the Supplementary Materials.

an inflammatory response that amplifies the original damage and, further, reveal novel potential targets to prevent this side-effect of chemotherapy.

INTRODUCTION

DNA damage is continually induced by environmental agents and chemically reactive by-products of normal cellular metabolism. Moreover, DNA damage is often deliberately induced during the course of cancer chemotherapy. One class of commonly used chemotherapeutics is a broad group of compounds called alkylating agents, which add alkyl groups to DNA. Alkylating agents generate numerous types of alkylated DNA base lesions, including O^6-methylguanine, 7-methylguanine (7meG) and 3-methyladenine (3meA). The efficacy of alkylators as cancer chemotherapeutic agents relies on the induction of cell death in rapidly dividing tumor cells by DNA lesions that interfere with DNA replication and RNA transcription. DNA repair pathways have evolved to cope with recurring DNA damage and, for the most part, provide protection in healthy tissues. The base excision repair (BER) pathway for alkylated DNA bases (1, 2) is initiated by the alkyladenine DNA glycosylase (AAG, also known as MPG), which recognizes and excises 7meG and 3meA, as well as etheno(ε)-DNA adducts (3, 4). ε-DNA adducts are produced endogenously by products of lipid peroxidation that occur under oxidative stress conditions, such as inflammation (5–8). After base excision, an apurinic/apyrimidinic endonuclease 1 (APE1) hydrolyzes the phosphodiester backbone at the abasic site, generating a single-stranded DNA break (SSB) with 3′OH and 5′deoxyribose-5-phosphate (5′dRP) termini (Fig. 1). DNA polymerase β (Pol β) removes the 5′dRP terminus and conducts single-nucleotide gap filling synthesis. BER is completed upon ligation of the nicked DNA by DNA ligase I or the XRCC1/ligase IIIα complex. Poly(ADP-ribose) polymerase 1 [PARP1, also known as ADP-ribosyltransferase 1 (ADPRT1) or ADP-ribosyltransferase diphtheria toxin-like 1 (ARTD1)] is a multifunctional protein that mediates several cellular processes and plays an important role in BER (9–18). PARP1 acts as a SSB sensor and, upon binding a SSB, is activated to use nicotinamide adenine dinucleotide (NAD^+) to catalyze the addition of long, branched polymers of ADP-ribose (PAR) to several nuclear proteins, including itself, DNA polymerases, DNA ligases, transcription factors, and histones (15, 19, 20). PARylation of histones, PARP1, and chromatin remodeling enzymes serves to relax chromatin, facilitating the access of DNA repair proteins to the damage (21–23). Moreover, PARP1 automodification is thought to recruit the BER scaffold protein XRCC1, which facilitates the formation of a complex of BER enzymes, including Pol β and DNA ligase III (Fig. 1) (24–26). With the completion of repair, PARP1 dissociates from the DNA and PAR is rapidly degraded, primarily by PAR glycohydrolase (27). Together, these functional aspects of PARP1 serve to facilitate BER, enabling cells to recover from DNA damage.

Although BER can efficiently complete the repair of DNA alkylation damage in most cells, in certain cell types, the initiation of BER can generate toxic repair intermediates that cause damage to healthy tissues (Fig. 1). We have previously shown that alkylating agents can induce BER-dependent retinal degeneration (RD) in mice (28–30). Specifically, we demonstrated the importance of both AAG and PARP1 in modulating in vivo alkylation-induced toxicity in the retina and found that this alkylation toxicity is sex dependent. The

alkylating agent, methyl methanesulfonate (MMS), induces photoreceptor (PR) degeneration in wild-type (WT) male mice, whereas WT female mice are partially protected (30, 31). Modest increases in AAG activity in a transgenic mouse model (*AagTg*) exacerbate, rather than suppress, retinal susceptibility to the alkylating agent. In the absence of AAG activity, the retina is totally refractory to MMS-induced PR cell death that is induced in both WT and *AagTg* mice (29). AAG-mediated alkylation sensitivity in the retina, in both WT and *AagTg* mice, is entirely PARP1 dependent, being wholly prevented by *Parp1* gene deletion and partially prevented by pharmacological PARP inactivation (29, 30).

Certain environmental or pathological conditions can trigger a regulated form of necrotic cell death, characterized by cytoplasmic swelling, vacuolization and rupture of the plasma membrane with subsequent stimulation of the inflammatory response [reviewed in (32–36)]. These triggers can initiate a diversity of potentially overlapping, yet distinct, necrotic cell death pathways (35). Although different necrotic cell death pathways are beginning to emerge, the protein factors and mechanisms that modulate the signaling and execution of the multiple necrotic cell death pathways remain to be fully elucidated, including their cell and tissue specificities.

Alkylating agents can trigger a regulated form of necrosis that is dependent on PARP1 hyperactivation (also known as parthanatos) (37–41). PARP1 can act as a cell death mediator (42, 43); upon excessive DNA damage, PARP1 hyperactivation vastly increases NAD^+ consumption, resulting in depletion of both NAD^+ and ATP, such that cells succumb to bioenergetic failure and necrotic cell death (42, 44, 45). Independent of NAD^+/ATP depletion, the PAR polymer can also inhibit mitochondrial hexokinase 1, thus blocking glycolysis with consequent energy collapse and cell death (46). The PAR polymer can also promote cell death by facilitating translocation of the apoptosis-inducing factor from mitochondria to the nucleus, resulting in chromatin condensation, caspase-independent DNA degradation, and ultimately, cell death (37, 47, 48).

Evidence indicates that necrosis can also be induced by regulated signal transduction pathways, such as those mediated by the receptor-interacting protein (RIP) kinases, RIP1 and RIP3 (49–51). This unique mechanism of cell death is termed necroptosis (52) and can be initiated by the Fas and tumor necrosis factor receptor family of death receptors or Toll-like receptors (TLRs) (51). RIP1 is a multifaceted death domain adaptor protein that mediates both apoptosis and necrosis. RIP1 stimulates apoptosis when recruited to the protein complex containing the Fas-associated death domain and caspase-8 (53, 54). When caspases are either inhibited or not activated, RIP1 binds to RIP3 to form a pronecrotic complex that interacts with and activates several metabolic enzymes that increase the production of reactive oxygen species (ROS), ultimately leading to membrane rupture and necrotic cell death (55–57). The pronecrotic complex also phosphorylates the pseudokinase mixed lineage kinase domain-like protein (MLKL), which is suggested to trigger necroptosis by binding to and initiating ion fluxes through cellular membranes (58–62).

Inflammation is known to be an important pathological feature of necrosis, independently of the mechanisms that trigger it (63). Inflammation can induce persistent oxidative stress through the production of reactive oxygen and nitrogen species (RONS) that can react with

polyunsaturated fatty acid residues of phospholipids initiating lipid peroxidation. Lipid peroxidation products are a major endogenous source of ε-DNA adducts (5–8), highly mutagenic base lesions characterized by an exocyclic (imidazole) ring. AAG-initiated BER is the major pathway for the repair of ε-DNA adducts (3, 4); therefore, alkylation-induced necrosis/inflammation, if present, would produce more substrates for AAG with consequent amplification of the inflammatory response and tissue damage.

We have previously shown that PARP1 hyperactivation modulates retinal cell death after alkylation-induced damage (29, 30, 64), whereas RIP kinase–dependent necroptosis has been shown to account for retinal cell death after inflammation, retinal detachment, and in the presence of specific genetic mutations (65–67). The RIP kinase–dependent pathway is either distinct from, or intertwined with, the PARP1 cell death pathway, depending on the cell type and the specific kind of stressor (68–71). To our knowledge, an extensive investigation of the mechanisms of alkylation-induced RD has not previously been reported, and apoptosis is assumed to be the main mechanism of alkylation-induced PR cell death (72–74). Here, we investigated a possible role for necrosis, RIP kinases, and inflammation in alkylation-induced PR degeneration. We identified RIP3 kinase–mediated necrosis and the activation of a robust inflammatory response as mechanisms of PR cell death in alkylation-induced PR degeneration, thus identifying potential therapeutic targets. Given the extensive use of alkylating agents as chemotherapeutics, understanding the molecular mechanisms underlying alkylation-induced PR cell death may be crucial to prevent potential side effects of cancer chemotherapy.

RESULTS

MMS induces AAG-dependent and sex-dependent morphological changes in the retina

Previously, we showed that the BER-initiating enzyme AAG drives alkylation-induced cytotoxicity in retinal PRs in WT mice (28, 29). The extent of alkylation-induced PR damage is sex dependent; WT males are more sensitive than are females (30). Seven days after MMS treatment, WT males have substantially fewer PR cell layers than WT females, whereas *Aag*$^{-/-}$ male mice are completely refractory to alkylation-induced PR degeneration. To determine the time course of alkylation-induced PR degeneration, and to further study the overall morphological changes in the retina, both male and female WT and *Aag*$^{-/-}$ mice were injected with MMS (75 mg/kg), and their retinas were examined at 3, 5, and 7 days after MMS treatment.

MMS induced selective degeneration of PR cells located in the outer nuclear layer (ONL) of the retina (Fig. 2), as was previously shown (28–30). PR degeneration was quantified by counting the rows of PR nuclei in the ONL on stained histological sections. For both genotypes, untreated male and female mice had about 11 rows of PR nuclei (Fig. 2, A and B). In WT mice, PR degeneration was evident at 3 days after MMS treatment and was similar in male and female mice (Fig. 2, A and B). PR degeneration increased over time in WT male mice, whereas no further degeneration was observed over time in WT female mice (Fig. 2, A and B). In *Aag*$^{-/-}$ mice, we observed no PR degeneration at any time point, regardless of gender (Fig. 2).

In addition to PR degeneration, we observed retinal pigment epithelium (RPE) cell lesions, consisting of swollen and vacuolated RPE cells, predominantly in WT male mice (Fig. 2A). Degeneration of RPE cells in male mice was patchy and evident in all samples starting at day 5 (Fig. 2A). In agreement with these findings, immunostaining for zona occludens-1 (ZO-1), a tight junction-associated protein expressed in the RPE cells, showed patchy, abnormal RPE topography in WT male mice (fig. S1A). However, no loss of RPE cells at day 5 after MMS treatment was observed (fig. S1A). In $Aag^{-/-}$ mice, we observed no RPE lesions at any time point, regardless of gender (Fig. 2).

We also observed abnormal cellular infiltrates between the ONL and RPE cell layer (subretinal space) in both male and female WT mice (white arrowheads in Fig. 2A). However, the frequency of infiltrate cells was significantly higher in male mice than in female mice (Fig. 2, A and C). No morphological alterations were observed in any other retinal layer. In MMS-treated $Aag^{-/-}$ mice, we observed no subretinal cellular infiltration at any time point, regardless of gender (Fig. 2). Together, our findings demonstrate that the retina displays AAG- and sex-dependent alkylation-induced morphological changes consisting of PR degeneration, RPE cell lesions, and abnormal cell infiltration into the subretinal space.

PR cells exhibit necrotic morphology after MMS-induced damage

We previously showed that AAG-mediated alkylation sensitivity of PRs is entirely PARP1 dependent, being wholly prevented by *Parp1* gene deletion and partially prevented by pharmacological PARP inactivation (30, 75). Several reports show that PARP1-dependent cell death occurs mainly by necrosis (39, 42, 44, 45). However, an extensive investigation of alkylation-induced retinal necrosis has not, to our knowledge, been reported, and apoptosis is still thought to be the main mechanism of alkylation-induced PR degeneration (72–74). To study the involvement of necrosis in the alkylation-induced PR degeneration, we investigated the presence of necrotic cell morphology in the retina after MMS injection. Male and female WT male mice were untreated or treated with MMS (75 mg/kg), and cell morphology was studied by electron microscopy (EM). Untreated WT mice showed no PR cell death (Fig. 3A). Three days after MMS injection, the degenerating PR layer (the ONL) exhibited the presence of both apoptotic and necrotic nuclei (Fig. 3A). Nuclei in the ONL showing chromatin condensation were defined as apoptotic, whereas nuclei showing karyolysis and discontinuity in the nuclear membrane were defined as necrotic. Electron-dense granular material reportedly occurs subsequent to both apoptotic and necrotic cell death and was labeled as unclassified (76, 77). The average percentage of PR death caused by necrosis was similar to that caused by apoptosis in both males and females (Fig. 3B) at day 3. However, the overall percentage of cell death was significantly reduced in female WT mice versus male WT mice, supporting our data above (Fig. 2). In addition, the PR outer segment (OS) and inner segment (IS) structures were severely damaged, exhibiting vacuoles, swollen/disrupted mitochondria, and ruptured plasma membranes and/or organelles, further supporting the presence of PR necrosis (Fig. 3C). Plasma membrane rupture is characteristic of necrotic cells, whereas apoptotic cells retain plasma membrane integrity. Consistent with EM analysis, intravitreal injections of propidium iodide (PI) to specifically label cells with disrupted cell membranes before removal of the eyes produced PI-positive PRs in the MMS-

treated WT mice (Fig. 3D) 3 days after MMS injection. The number of PI-labeled PRs was significantly higher in male than female WT mice (Fig. 3, D and E), and no PI-stained PRs were detected in MMS-treated *Aag*$^{-/-}$ mice, as expected.

Unlike PRs, RPE cell analysis by EM did not show apoptotic or necrotic nuclei but did show swollen RPE cells and cytoplasmic vacuoles (fig. S1B), confirming the H&E results (Fig. 2). Overall, our data show that MMS specifically induces PR cell death by both necrosis and apoptosis.

PRs exhibit increased MMS-induced expression of necroptotic markers, Rip1 and Rip3

RIP3 is a key regulator of RIP1 kinase activation (51). The abundance of RIP3 is correlated with responsiveness to programmed necrosis (56). We therefore studied the expression of *Rip3* and *Rip1* mRNA in the neural retina 3 days after MMS injection by quantitative real-time polymerase chain reaction (PCR). *Rip3* gene expression was increased nearly 35-fold in the neural retina of MMS-treated WT male mice versus that in untreated mice (Fig. 4). *Rip1* expression was only increased about threefold (Fig. 4). Enzyme-linked immunosorbent assay (ELISA) for RIP3 confirmed that RIP3 protein expression was increased after MMS treatment (fig. S2A). In WT male mice, increased *Rip1* and *Rip3* expression was accompanied by MLKL phosphorylation, an RIP3 substrate (fig. S2B). MMS induced *Rip3* expression by 15.1-fold in the neural retina of WT female mice, which was notably less than that observed in WT male mice; the increased amount of MMS-induced *Rip1* expression was similar in both sexes (2.2-fold in females and 2.8-fold in males; Fig. 4). No increase of either *Rip1* or *Rip3* expression was observed in *Aag*$^{-/-}$ or *Parp1*$^{-/-}$ mice after treatment with MMS (Fig. 4 and fig. S2C). Together, our data suggest that RIP-mediated necrosis is involved in the specific PR loss seen after MMS treatment.

MMS treatment increases oxidative stress

Oxidative damage has been implicated in PARP1-dependent necrosis (42, 44, 45). Moreover, it has been demonstrated that the RIP3 kinase stimulates necrosis by overproduction of ROS in several cell types (55, 78, 79). Likewise, inflammation can induce persistent production of RONS. RONS can react with DNA, generating 8-hydroxyguanine (8-oxoG), along with other DNA base lesions. We therefore determined whether MMS treatment results in RONS-induced oxidative DNA damage, using 8-oxoG as a biomarker of such damage. Staining for 8-oxoG confirmed that PR cells in MMS-treated WT male mice accrue substantial levels of oxidative DNA damage, presumably because MMS induces increased levels of cellular RONS (Fig. 5). 8-oxoG staining was undetectable in untreated mice and in MMS-treated *Aag*$^{-/-}$ mice.

MMS induces an AAG-dependent retinal inflammatory response

Inflammation is an important pathological feature of necrosis. Dying necrotic cells release damage-associated molecular pattern (DAMP) proteins into the extracellular space, which activate the innate immune response by interacting with cellular receptors, such as TLRs (80). High-mobility group box 1 (HMGB1), an abundant nuclear protein, is a major DAMP protein released from necrotic cells (81–83). It has been shown that, after alkylation damage, the activation of PARP1 regulates HMGB1's translocation from the nucleus to the cytosol

(39, 84). This displaced HMGB1 is subject to release because the cells lose plasma membrane integrity during necrosis. We therefore examined PARP1 activity and HMGB1 levels in the PRs after MMS treatment. Three days after MMS treatment, PARylation was markedly increased in the retina of MMS-treated WT male mice, compared to untreated mice, and was largely localized to the PR nuclei (Fig. 6 and fig. S3). As expected (28–30), PARylation was muted in WT female mice (fig. S3) and was absent in *Aag*$^{-/-}$ mice (Fig. 6 and fig. S3) in accordance with the amount of PR degeneration after alkylation damage (Fig. 2). In untreated WT male mice, HMGB1 was localized to the nucleus of several cells, including the PRs (Fig. 6). Three days after treatment with MMS, HMGB1 was specifically absent from PR nuclei (Fig. 6). The absence of HMGB1 in the PR nucleus was associated with the presence of PARylation, consistent with the activation of PARP1 inducing the release of HMGB1. As expected, by the absence of PARylation, no HMGB1 release was observed in MMS-treated *Aag*$^{-/-}$ mice (Fig. 6).

Both the activation of PARP1 and the release of HMGB1 have been associated with the induction of an innate immune inflammatory response (17, 18, 81, 85); we therefore analyzed the activation and recruitment of inflammatory cells to the site of the damage after MMS treatment. Immunofluorescence for the microglial marker Iba1 on retinal flat mounts of untreated WT male mice showed a dense network of ramified microglial cells in the inner plexiform layer (IPL) and the absence of microglial cells in and around the ONL (Fig. 7A). In WT male mice at 5 days after MMS treatment, we observed that activated ameboid microglial cells with retracted processes and rounded cell bodies were present in the IPL, along with a remarkable migration of these cells into and around the ONL, the region where necrotic PR cell damage occurs. Such mobilization of the glial cells, called gliosis, is commonly accompanied by the up-regulation of the glial fibrillary acidic protein (GFAP), an intermediate filament protein, in the processes of Müller cells that extend toward the distal margins of the retina. GFAP was up-regulated in MMS-treated WT male retinas compared to untreated retinas at day 3 after treatment (Fig. 7B). Moreover, staining for F4/80, a marker for macrophages, showed that the subretinal space and the ONL were invaded by macrophages at day 3 after MMS treatment in WT male mice (Fig. 7C), in agreement with the histological results above (Fig. 2). Microglial activation and macrophage recruitment were reduced in MMS-treated WT females compared to MMS-treated WT males and were notably absent in MMS-treated *Aag*$^{-/-}$ mice (Fig. 7).

We also evaluated the expression levels of both proinflammatory and anti-inflammatory markers in the neuroretina 3 days after MMS treatment. The mRNA expression of proinflammatory cytokines encoded by the genes *Tnf-α* and *Il1*β, and that of the proinflammatory chemokine encoded by *Mcp-1/Ccl2*, an essential mediator of gliosis and macrophage infiltration, were increased 78.7-fold, 7.4-fold, and 386.8-fold, respectively, in the neuroretina of WT male mice after MMS treatment, compared to untreated WT male mice (Fig. 8). Along with increases in proinflammatory markers, we also observed increased transcription of the anti-inflammatory cytokine *Il10* in the neural retina of WT male mice after MMS treatment, compared to untreated controls (27-fold; Fig. 8). In WT female mice, mRNA expression of genes encoding pro- and anti-inflammatory markers showed similar or slightly reduced MMS-induced changes compared to WT males (*Tnf-α*, 51.2-fold; *Il1*β, 4-fold; *Mcp-1/Ccl2*, 325.4-fold; *Il10*, 27.6-fold), whereas no changes in those were observed

in MMS-treated *Aag*$^{-/-}$ mice (Fig. 8). These data suggest that the release of intracellular DAMP molecules and the induction of an inflammatory response in the ONL are involved in AAG- and sex-dependent alkylation-induced PR degeneration.

Together, our findings indicate that the AAG-dependent response of PR cells to alkylation damage triggers necrosis that is more robust in males than in females and an inflammatory response that is slightly muted in females compared to males. The inflammatory response might, in turn, generate more DNA damage, which can be acted upon by the AAG glycosylase, triggering further necrosis in males and, thus, establishing a vicious cycle.

RIP3 deficiency protects both males and females against MMS-induced RD and inflammation

We observed an AAG-dependent MMS-induced increase in both mRNA and protein abundance for the kinase RIP3, which is known to be involved in programmed necrosis. Therefore, we examined the effect of RIP3 deficiency on alkylation-induced PR degeneration. Male and female WT and *Rip3*$^{-/-}$ mice were exposed to MMS, and their retinas were analyzed at 3 and 7 days after treatment. Untreated male and female *Rip3*$^{-/-}$ mice had about 11 rows of PR nuclei, similar to that in WT mice (Fig. 9, A and B). In MMS-treated WT male mice, the number of rows of PR nuclei decreased to about seven by day 3, further decreasing to three by day 7, as expected (Figs. 9, A and B, and Fig. 2). In MMS-treated *Rip3*$^{-/-}$ male mice, the number of rows of PR nuclei dropped to 7 by day 3, similar to MMS-treated WT male mice. However, no further progression of the degeneration was observed by day 7, and the number of rows of PR nuclei was significantly higher in MMS-treated *Rip3*$^{-/-}$ male mice versus WT mice on day 7, indicating that *Rip3* deficiency partially protects against alkylation/inflammation-induced PR degeneration. In MMS-treated WT female mice, the rows of PR nuclei decreased to seven by day 3 and remained stable through day 7, as expected (Figs. 9, A and B, and 2). In MMS-treated female mice, the number of rows of PR nuclei remained slightly higher on days 3 and 7 in *Rip3*$^{-/-}$ mice versus WT mice (Fig. 9, A and B), suggesting that *Rip3* deficiency modestly protects females against alkylation/inflammation-induced PR degeneration. Moreover, in both male and female *Rip3*$^{-/-}$ mice treated with MMS, the number of cells infiltrating the subretinal space was significantly lower than that observed in the WT counterpart mice (Fig.9, A to C), indicating that the absence of *Rip3* reduces the inflammatory response. The number of PI-positive PRs in the MMS-treated *Rip3*$^{-/-}$ male mice was reduced compared to MMS-treated WT mice (fig. S4A), and we did not observe a statistically significant increase in the inflammatory markers, *Tnf-α* and *Mcp-1/Ccl2* (fig. S4B), further confirming that *Rip3* deficiency partially protects against MMS-induced necrosis and inflammation.

Deficiency of IL-10 increases AAG-dependent MMS-induced RD in both males and females

We observed an AAG-dependent MMS-induced increase in the transcript for interleukin-10 (IL-10), an anti-inflammatory cytokine. We therefore examined the role of IL-10 in alkylation-induced PR degeneration. Retinas from male and female WT, *Il10*$^{-/-}$, and *Aag*$^{-/-}$/*Il10*$^{-/-}$ mice were analyzed 7 days after MMS treatment. Untreated mice of all genotypes and both sexes had about 11 rows of PR nuclei (Fig. 10, A and B). After MMS treatment, the ONL of WT male mice was significantly more damaged compared to that in WT female

mice (Figs. 10, A and B, and 2), as expected (30). Both male and female MMS-treated *Il10*$^{-/-}$ mice showed greater PR degeneration than did MMS-treated WT mice (Fig. 10, A and B), indicating that an anti-inflammatory cytokine influences the extent of AAG-dependent alkylation-induced RD, supporting our conclusion that inflammation plays a role in the degenerative process. Male and female *Aag*$^{-/-}$/*Il10*$^{-/-}$ were completely refractory to MMS-induced degeneration, consistent with AAG being responsible for initiating the degenerative cascade of events.

Pan-caspase inhibitor partially protects WT female, but not male, mice against MMS-induced RD

Using EM, we observed both necrosis and apoptosis in MMS-treated WT mice. To evaluate the relative contribution of apoptosis to MMS-induced PR cell death, we inhibited apoptosis in male and female WT mice with Q-VD-Oph (10 mg/kg), a pan-caspase inhibitor. Q-VD-Oph was administered just before and again at 24 hours after MMS injection, and retinas were analyzed 7 days after treatment. Whereas Q-VD-Oph did not protect WT male mice against alkylation-induced degeneration, it partially protected WT female mice (Fig. 11, A and B). Q-VD-Oph or its vehicle alone were not toxic and did not induce any RD (Fig. 11 and fig. S5B). In this particular set of experiments, we observed more severe MMS-induced RD in both male and female WT mice, compared to the data described above (Figs. 2, 9, and 10). Nevertheless, female mice were less sensitive than male mice to MMS-induced RD (Fig. 11), consistent with the trend in those aforementioned data. The more severe MMS-induced RD in this experiment might be due to differences in MMS batches used. As for WT male mice, Q-VD-Oph did not rescue *Rip3*$^{-/-}$ male mice from alkylation-induced degeneration (fig. S5). Together, the data suggest that, in male mice, the predominant mechanism of MMS- and inflammation-induced cell death is necrosis.

Discussion

In this study, we demonstrated that programmed necrosis and subsequent inflammation are important mediators of AAG-dependent alkylation-induced PR cell loss in male mice. RIP3-mediated necrosis, also known as necroptosis, and PARP1-mediated necrosis are the most extensively studied mechanisms of programmed necrosis (37–41, 86). We previously showed that alkylation-induced PR degeneration is initiated by AAG and is entirely PARP1 dependent, being wholly prevented by either *Aag* or *Parp1* gene deletion, and partially prevented by pharmacological PARP inactivation (28–30), suggesting that PARP1-mediated necrosis (downstream from AAG) is involved in alkylation-induced PR cell death. Oxidative damage has been implicated in PARP1-mediated necrosis (42, 44, 45). Moreover, it is known that activation of PARP1 regulates the release of HMGB1 as a DAMP molecule (39, 84) and that extracellular PAR also acts as a DAMP molecule driving inflammatory signaling for the recruitment of macrophages (87). We showed that PR cells present necrotic morphology and oxidative DNA damage after the induction of PR cell death with alkylating agents; furthermore, we observed that PARylation in the PR nuclei is associated with the release of HMGB1, increased macrophage infiltration, and elicitation of an inflammatory response. This study unveils the mechanism of alkylation-induced PR cell death and

underscores the importance of PARP1-mediated necrosis and inflammation in alkylation-induced RD.

In addition to PARP1-mediated necrosis, RIP kinase–mediated necroptosis also plays an important role in AAG-dependent alkylation-induced PR cell loss in male mice. The expression levels of retinal *Rip1* and *Rip3* are increased after alkylation exposure in WT, but not in $Aag^{-/-}$, male mice. Moreover, *Rip3* deletion partially protects WT mice from alkylation-induced PR cell loss, attenuating necrosis and reducing inflammation. Necroptosis has been shown to be critical for various retinal diseases (65–67). The primary inducer of necroptosis is the death receptor, tumor necrosis factor receptor 1 (TNF-R1). The binding of TNF to TNF-R1 induces the activation of RIP1/RIP3. This activation triggers a panoply of effector mechanisms, including glycogenolysis, glutaminolysis, the formation of ROS, mitochondrial dysfunction, and membrane rupture upon phosphorylation of MLKL and its insertion into plasma membranes, all culminating in necroptotic cell death (34, 88). Initial studies have implicated the PARP pathway as an integral part of necroptosis (51, 89). PARP1 has been shown to be activated by RIP1 and RIP3 and to contribute to the necroptotic phenotype by reducing ATP levels (51, 89). However, a study showed that necroptosis and PARP1-mediated necrosis represent distinct and independent routes to programmed necrosis (71). We observed no increased RIP1 or RIP3 expression in MMS-treated $Parp1^{-/-}$ mice (fig. S2C), suggesting that necroptosis is dependent on PARP1 activation in this model. Moreover, we observed total protection against alkylation-induced PR degeneration in $Parp1^{-/-}$ mice (29, 30), whereas $Rip3^{-/-}$ mice were only partial protected, suggesting that inhibition of necroptosis is not sufficient to fully protect against alkylation-induced RD, further supporting the hypothesis that activation of necroptosis might be secondary to PARP1 activation. PARP1 has been shown to increase the expression of several cytokines (90), including TNFα; therefore, necroptosis might be a consequence of PARP1-induced TNFα expression. Nevertheless, whether the pathways are interconnected or separated in our model will require further studies. Studies have shown that, independently of cell death signaling, RIP1 and RIP3 fulfill additional signaling functions, including activation of the inflammasome and production of inflammatory cytokines (92–97). Therefore, we do not exclude that the protective effect of *Rip3* gene deletion against alkylation-induced PR loss might be due to decreased necroptosis, decreased RIP3-induced inflammation, or a combination of both. At present, it is not possible to separate the effect of RIP3-induced inflammation from those of necroptosis and the release of DAMPs, especially because, in at least one case, the RIP3-mediated proinflammatory effect was observed to also depend on MLKL, a crucial effector of necroptosis (98), which we have shown to be phosphorylated in the retinas of MMS-treated mice. However, the distinction may not ultimately be important in the clinic, because interference with RIP3 activation and function will likely have therapeutic benefits, regardless of the precise pathological mechanism of alkylation-induced tissue damage.

It is important to stress that AAG-dependent alkylation-induced cell death is cell-type specific (29, 64). We observed alkylation-induced cell death only in the PR cells but not in other retinal cell types. One possible explanation for alkylation-induced selective damage in the PRs is that alkylating agents preferentially target cells with higher energy demands. The OS discs of the PRs, the place where the phototransduction cascade occurs, are exposed to

constant photo-oxidative stress and go through constant destruction and renewal. However, we do not exclude the possibility that AAG might be differently expressed in different retinal cell types, resulting in a differential ability to activate PARP1 and to undergo to cell death.

In addition to programmed necrosis, we have also observed apoptosis in PR cells after treatment with alkylating agents, suggesting that alkylation toxicity in the PRs might be caused by differential contribution of multiple cell death pathways. Moreover, female mice are partially resistant to PR cell death, and treatment with Q-VD-Oph, a pan-caspase inhibitor, partially protects WT female, but not male, mice against alkylation-induced PR death. These data suggest that PRs in male and female mice display a sex-specific bias for distinct cell death pathways, with male mice being more prone to necrotic cell death. It has been shown that neurons that have two X chromosomes, versus X and Y chromosomes, display different sensitivities to cytotoxic agents, with females' neurons being more sensitive than males' to apoptosis-inducing agents, and males' neurons being more sensitive than females' to nitrosation-induced necrotic cell death (99). In addition, *Parp1* deficiency was shown to protect male, but not female, animals against cerebral ischemia and autoimmune nephritis (100–105), and treatment with Q-VD-Oph resulted in reduced cerebral infarction in females but not in males (103), further suggesting a bias for distinct cell death pathways between the sexes.

We found that inflammation plays an important role in AAG-dependent alkylation-induced PR cell loss. It seems likely that inflammation is secondary to PARP1- and/or RIP3-dependent necrosis initiated by the action of AAG on DNA alkylation damage, being elicited by the release of DAMP molecules, although it is possible that activated PARP1 and RIP3 might also directly induce inflammation. Once triggered, inflammation creates persistent oxidative stress and lipid peroxidation, which, in turn, can cause accumulation of ε-DNA adducts (5–8), leading to further AAG-dependent PARP1 activation that further amplifies the inflammatory response and magnifies tissue damage. Inflammation after alkylation was also accompanied by increased anti-inflammatory IL-10 expression, and deletion of the *Il10* gene resulted in increased PR loss, suggesting that IL-10 plays a protective role against alkylation-induced RD, and further supporting our conclusion that inflammation plays a role in the degenerative process. Mice deficient in both *Aag* and *Il10* were completely refractory to MMS-induced RD, consistent with AAG being solely responsible for initiating the degenerative cascade of events.

Conspicuously, whereas it is clear that the effect of the alkylation-induced cell death is much stronger in females compared to males, the overall alkylation-induced inflammatory response appears to be only slightly reduced in female mice compared to males. The inflammatory response seen in female mice might not be secondary to PARP1- and/or RIP3-dependent necrosis initiated by the action of AAG, as discussed above, but due to the ability of the activated PARP1 and RIP3 to directly induce inflammation (17, 90–97), or to some other unknown mechanism that will need to be clarified.

Our findings show that AAG-initiated BER at alkylated DNA bases induces sex-dependent PR degeneration mainly by triggering programmed necrosis and activating a robust

inflammatory response. Given the extensive use of alkylating agents as chemotherapeutics and exposure to such agents in natural and man-made environments, understanding the molecular mechanisms underlying alkylation-induced PR cell death may be crucial to the identification of novel targets for the prevention of RD.

Materials and Methods

Animals and treatments

Rip3$^{-/-}$ mice were a gift from D. Vavvas (Massachusetts Eye and Ear Infirmary, Boston, MA) and were previously described (106). *Parp1*$^{-/-}$ (the Jackson Laboratory) and *Aag*$^{-/-}$ mice were described previously (107, 108). WT, *Aag*$^{-/-}$, and *Rip3*$^{-/-}$ mice were all on a C57BL6 genetic background. *Parp1*$^{-/-}$ mice were on a mixed background (C57Bl/6J:129S). All animal procedures were performed in accordance with the National Institutes of Health guide for the Care and Use of Laboratory Animals.

MMS (75 mg/kg; Sigma) and Q-VD-Oph (10 mg/kg; ApexBio) were administered by intraperitoneal injections. Q-VD-Oph was administered right before and 24 hours after MMS injection.

Histological analysis

Eyes were fixed in Carnoy's fixative for 24 hours. Tissues were processed by the Histology Core Facility at the David H. Koch Institute for Integrative Cancer Research (Massachusetts Institute of Technology); they were paraffin-embedded, sectioned at 5 μm, and stained with H&E. All H&E-stained slides were blindly analyzed using a Nikon Eclipse 6800 microscope, a Retiga Exi camera, and Velocity and ImageJ software.

To quantify RD, the number of rows of PR nuclei in the ONL of each eye was counted. A minimum of three sections, close to the optic nerve area, were analyzed for each eye. For each section, the number of rows of PR nuclei in the ONL was counted at three different points along the retina and averaged. The averaged counts for each of the three sections were then averaged for each eye. All eyes in an experimental group were then averaged and standard errors were calculated.

To quantify subretinal cell infiltration, the number of ectopic nuclei between the RPE and PR ONL was counted on eye sections containing the optic nerve. Counts from at least three different sections close to the optic nerve were averaged for each eye.

Electron microscopy

Tissue processing and imaging were performed by the W.M. Keck Microscopy Facility at the Whitehead Institute (MIT). Eyes were fixed in 2.5% gluteraldehyde and 3% paraformaldehyde (PFA) with 5% sucrose in 0.1 M sodium cacodylate buffer (pH 7.4), postfixed in 1% osmium tetroxide in veronal-acetate buffer, stained overnight with 0.5% uranyl acetate in veronal-acetate buffer (pH 6.0), and then embedded in EMbed 812 resin. Ultrathin sections were cut from blocks on a Leica Ultracut UCT microtome with a Diatome diamond knife. The sections were blindly examined using an FEI Tecnai Spirit at 80 keV. More than 150 to 200 PRs per eye were photographed, and cell death type was quantified in

a masked fashion. PR nuclei showing nuclear condensation were defined as apoptotic nuclei, whereas PR nuclei showing kariolysis and discontinuity in the nuclear membrane were defined as necrotic. Electron-dense granular materials were labeled as unclassified because these materials are reported to occur subsequent to both apoptotic and cell death (76, 77, 109, 110).

In vivo PI staining

Five microliters of PI (50 μg/ml) was injected in the vitreous 3 days after MMS injection. After 2 hours, the eyes were enucleated, fixed in 4% PFA and subsequently embedded in optimal cutting temperature compound. Nuclei on cryosections were counterstained with DAPI. PI-stained PR nuclei were blindly quantified on at least three sections per eye and adjusted to the number of cells per square millimeter of ONL using the ImageJ software.

Flat-mount staining

Eyes were enucleated and fixed in 4% PFA for 4 hours. After washing with phosphate-buffered saline (PBS), the anterior segment was removed and the neuroretina was separated from RPE/choroid-sclera under a microscope. The neuroretina was incubated in blocking buffer [2.5% bovine serum albumin (BSA), 0.3% Triton X-100, and 3% serum in PBS] for 2 hours and then further incubated with an antibody for Fc receptor (1:100; catalog number 553141, BD Pharmigen) for 45 min, followed by incubation with an antibody for Iba1 (1:200; catalog number 019–19741, Wako) overnight at 4°C and Alexa Fluor 568 (1:200; Invitrogen). Images were acquired with the Zeiss 700 laser scanning confocal microscope and ZEN 2010 software. The RPE/choroid-sclera was blocked with 10% nonfat dry milk and 0.3% Triton X-100 for 2 hours, and then incubated overnight with an antibody for ZO-1 (1:100; catalog number 617300, Thermo Fisher Scientific) at 4°C. Samples were consequently incubated with Alexa Fluor 594 (1:200; Invitrogen). Four to five areas were photographed at ×400 magnification with a Nikon Eclipse 6800 microscope, a Retiga Exi camera, and Velocity software. RPE cells were blindly counted using the ImageJ software and averaged.

Immunostaining

Deparaffinized tissue sections (5 μm) were permeabilized in PBS-T (1× PBS + 0.1% Triton X-100, three times for 5 min each), incubated with 5% BSA for 1 hour, and then stained for PAR (1:1000; catalog number 4335-MC-100, Invitrogen), HMGB1 (1:500; Ab18256, Abcam), 8-oxoG (1:200; Ab62623, Abcam), GFAP (1:500; Ab7779, Abcam), F4/80 (1:500; Ab6640, Abcam) or anti-pMLKL (1:200; Ab196436, Abcam) overnight at 4°C. After incubation with the secondary antibody conjugated with Alexa Fluor 488 or Alexa Fluor 568 (1:400; Invitrogen), nuclear counterstaining was performed using DAPI. Images were blindly analyzed using a Nikon Eclipse 6800 microscope, a Retiga Exi camera, and Velocity and ImageJ software.

Gene expression analysis

Eyes were enucleated and, after washing with PBS, the anterior segment was removed, and the neuroretina was separated from RPE/choroid-sclera under a microscope. RNA was

extracted from neuroretina using the RNeasy Mini Kit (Qiagen), and first-strand complementary DNA was synthesized using the SuperScript III First-Strand Synthesis System (Invitrogen), according to the manufacturer's instructions. Quantitative real-time PCR was performed using the 7500 Fast Real-Time PCR machine (Applied Biosystems) with TaqMan primers and probes (Invitrogen: *Rip3*, Mm00444947_m1; *Rip1*, Mm00436354_m1; *Tnf-α*, Mm00443258_m1; *Mcp-1/Ccl2*, Mm00441242_m1; *Il1*β, Mm00434228_m1; *Il10*, Mm01288386_m1). *Gapdh* was used as a housekeeping gene (Mm99999915_g1; Invitrogen).

Protein quantification by ELISA

RIP3 protein contents in retinal extracts were determined using ELISA kits (Cloud-Clone, SEE639Mu), according to the manufacturer's instructions.

Statistics

Statistical analyses were performed using the GraphPad Prism software. When several conditions were compared, one- or two-way ANOVA was performed, followed by Tukey's range test to assess the significance among pairs of conditions. When only two conditions were tested, statistical significance was determined using unpaired t tests. A *P* value was considered significant if less than 0.05.

Supplementary Material

Refer to Web version on PubMed Central for supplementary material.

Acknowledgments:

We thank the Hope Babette Tang Histology Core at the David H. Koch Institute for Integrative Cancer Research, N. Watson from W.M. Keck Microscopy Facility at the Whitehead Institute for technical help and S. Muthupalani for help with the EM analysis.

Funding: This work was supported by NIH grants R01-CA075576, R01-CA055042, P30-ES02109, and P30-CA014051. L.D.S. is an American Cancer Society Research professor and an Ellison Medical Foundation Senior scholar.

References and Notes:

1. Fu D, Calvo JA, Samson LD, Balancing repair and tolerance of DNA damage caused by alkylating agents. Nat Rev Cancer 12, 104–120 (2012). [PubMed: 22237395]
2. Robertson AB, Klungland A, Rognes T, Leiros I, DNA repair in mammalian cells: Base excision repair: the long and short of it. Cell Mol Life Sci 66, 981–993 (2009). [PubMed: 19153658]
3. Saparbaev M, Kleibl K, Laval J, Escherichia coli, Saccharomyces cerevisiae, rat and human 3-methyladenine DNA glycosylases repair 1,N6-ethenoadenine when present in DNA. Nucleic Acids Res 23, 3750–3755 (1995). [PubMed: 7479006]
4. Lee CY, Delaney JC, Kartalou M, Lingaraju GM, Maor-Shoshani A, Essigmann JM, Samson LD, Recognition and processing of a new repertoire of DNA substrates by human 3-methyladenine DNA glycosylase (AAG). Biochemistry 48, 1850–1861 (2009). [PubMed: 19219989]
5. el Ghissassi F, Barbin A, Nair J, Bartsch H, Formation of 1,N6-ethenoadenine and 3,N4-ethenocytosine by lipid peroxidation products and nucleic acid bases. Chem Res Toxicol 8, 278–283 (1995). [PubMed: 7766812]

6. Sodum RS, Chung FL, 1,N2-ethenodeoxyguanosine as a potential marker for DNA adduct formation by trans-4-hydroxy-2-nonenal. Cancer Res 48, 320–323 (1988). [PubMed: 3335007]
7. Sodum RS, Chung FL, Stereoselective formation of in vitro nucleic acid adducts by 2,3-epoxy-4-hydroxynonanal. Cancer Res 51, 137–143 (1991). [PubMed: 1703030]
8. Winczura A, Zdzalik D, Tudek B, Damage of DNA and proteins by major lipid peroxidation products in genome stability. Free Radic Res 46, 442–459 (2012). [PubMed: 22257221]
9. Lan L, Nakajima S, Oohata Y, Takao M, Okano S, Masutani M, Wilson SH, Yasui A, In situ analysis of repair processes for oxidative DNA damage in mammalian cells. Proc Natl Acad Sci U S A 101, 13738–13743 (2004). [PubMed: 15365186]
10. Caldecott KW, Single-strand break repair and genetic disease. Nature reviews. Genetics 9, 619–631 (2008).
11. Dantzer F, de La Rubia G, Menissier-De Murcia J, Hostomsky Z, de Murcia G, Schreiber V, Base excision repair is impaired in mammalian cells lacking poly(ADP-ribose) polymerase-1. Biochemistry 39, 7559–7569 (2000). [PubMed: 10858306]
12. Fisher AE, Hochegger H, Takeda S, Caldecott KW, Poly(ADP-ribose) polymerase 1 accelerates single-strand break repair in concert with poly(ADP-ribose) glycohydrolase. Mol Cell Biol 27, 5597–5605 (2007). [PubMed: 17548475]
13. Woodhouse BC, Dianova II, Parsons JL, Dianov GL, Poly(ADP-ribose) polymerase-1 modulates DNA repair capacity and prevents formation of DNA double strand breaks. DNA Repair (Amst) 7, 932–940 (2008). [PubMed: 18472309]
14. Lavrik OI, Prasad R, Sobol RW, Horton JK, Ackerman EJ, Wilson SH, Photoaffinity labeling of mouse fibroblast enzymes by a base excision repair intermediate. Evidence for the role of poly(ADP-ribose) polymerase-1 in DNA repair. J Biol Chem 276, 25541–25548 (2001). [PubMed: 11340072]
15. Schreiber V, Dantzer F, Ame JC, de Murcia G, Poly(ADP-ribose): novel functions for an old molecule. Nat Rev Mol Cell Biol 7, 517–528 (2006). [PubMed: 16829982]
16. Krishnakumar R, Gamble MJ, Frizzell KM, Berrocal JG, Kininis M, Kraus WL, Reciprocal Binding of PARP-1 and Histone H1 at Promoters Specifies Transcriptional Outcomes. Science 319, 819–821 (2008). [PubMed: 18258916]
17. Bai P, Virág L, Role of poly(ADP-ribose) polymerases in the regulation of inflammatory processes. FEBS Letters 586, 3771–3777 (2012). [PubMed: 23022557]
18. Luo X, Kraus WL, On PAR with PARP: cellular stress signaling through poly(ADP-ribose) and PARP-1. Genes Dev 26, 417–432 (2012). [PubMed: 22391446]
19. Satoh MS, Lindahl T, Role of poly(ADP-ribose) formation in DNA repair. Nature 356, 356–358 (1992). [PubMed: 1549180]
20. Kraus WL, Lis JT, PARP goes transcription. Cell 113, 677–683 (2003). [PubMed: 12809599]
21. Ahel D, Hořejší Z, Wiechens N, Polo SE, Garcia-Wilson E, Ahel I, Flynn H, Skehel M, West SC, Jackson SP, Owen-Hughes T, Boulton SJ, Poly(ADP-ribose)–Dependent Regulation of DNA Repair by the Chromatin Remodeling Enzyme ALC1. Science 325, 1240–1243 (2009). [PubMed: 19661379]
22. Timinszky G, Till S, Hassa PO, Hothorn M, Kustatscher G, Nijmeijer B, Colombelli J, Altmeyer M, Stelzer EHK, Scheffzek K, Hottiger MO, Ladurner AG, A macrodomain-containing histone rearranges chromatin upon sensing PARP1 activation. Nat Struct Mol Biol 16, 923–929 (2009). [PubMed: 19680243]
23. Gottschalk AJ, Timinszky G, Kong SE, Jin J, Cai Y, Swanson SK, Washburn MP, Florens L, Ladurner AG, Conaway JW, Conaway RC, Poly(ADP-ribosyl)ation directs recruitment and activation of an ATP-dependent chromatin remodeler. Proc. Natl. Acad. Sci. USA 106, 13770–13774 (2009). [PubMed: 19666485]
24. El-Khamisy SF, Masutani M, Suzuki H, Caldecott KW, A requirement for PARP-1 for the assembly or stability of XRCC1 nuclear foci at sites of oxidative DNA damage. Nucleic Acids Research 31, 5526–5533 (2003). [PubMed: 14500814]
25. Masson M, Niedergang C, Schreiber V, Muller S, Menissier-de Murcia J, de Murcia G, XRCC1 Is Specifically Associated with Poly(ADP-ribose) Polymerase and Negatively Regulates Its Activity following DNA Damage. Mol. Cell. Biol 18, 3563–3571 (1998). [PubMed: 9584196]

26. Vidal AE, Boiteux S, Hickson ID, Radicella JP, XRCC1 coordinates the initial and late stages of DNA abasic site repair through protein-protein interactions. Embo J 20, 6530–6539 (2001). [PubMed: 11707423]
27. Mortusewicz O, Fouquerel E, Ame JC, Leonhardt H, Schreiber V, PARG is recruited to DNA damage sites through poly(ADP-ribose)- and PCNA-dependent mechanisms. Nucleic Acids Res 39, 5045–5056 (2011). [PubMed: 21398629]
28. Meira LB, Moroski-Erkul CA, Green SL, Calvo JA, Bronson RT, Shah D, Samson LD, Aag-initiated base excision repair drives alkylation-induced retinal degeneration in mice. Proc Natl Acad Sci U S A 106, 888–893 (2009). [PubMed: 19139400]
29. Calvo JA, Moroski-Erkul CA, Lake A, Eichinger LW, Shah D, Jhun I, Limsirichai P, Bronson RT, Christiani DC, Meira LB, Samson LD, Aag DNA glycosylase promotes alkylation-induced tissue damage mediated by Parp1. PLoS Genet 9, e1003413 (2013). [PubMed: 23593019]
30. Allocca M, Corrigan JJ, Fake KR, Calvo JA, Samson LD, PARP inhibitors protect against sex- and AAG-dependent alkylation-induced neural degeneration. Oncotarget 8, 68707–68720 (2017). [PubMed: 28978150]
31. Jordan JJ, Chhim S, Margulies CM, Allocca M, Bronson RT, Klungland A, Samson LD, Fu D, ALKBH7 drives a tissue and sex-specific necrotic cell death response following alkylation-induced damage. Cell Death Dis 8, e2947 (2017). [PubMed: 28726787]
32. Pasparakis M, Vandenabeele P, Necroptosis and its role in inflammation. Nature 517, 311–320 (2015). [PubMed: 25592536]
33. Galluzzi L, Kepp O, Krautwald S, Kroemer G, Linkermann A, Molecular mechanisms of regulated necrosis. Semin Cell Dev Biol 35, 24–32 (2014). [PubMed: 24582829]
34. Vanden Berghe T, Linkermann A, Jouan-Lanhouet S, Walczak H, Vandenabeele P, Regulated necrosis: the expanding network of non-apoptotic cell death pathways. Nat Rev Mol Cell Biol 15, 135–147 (2014). [PubMed: 24452471]
35. Conrad M, Angeli JP, Vandenabeele P, Stockwell BR, Regulated necrosis: disease relevance and therapeutic opportunities. Nat Rev Drug Discov 15, 348–366 (2016). [PubMed: 26775689]
36. Newton K, Manning G, Necroptosis and inflammation. Annu Rev Biochem 85, 743–763 (2016). [PubMed: 26865533]
37. Yu SW, Wang H, Poitras MF, Coombs C, Bowers WJ, Federoff HJ, Poirier GG, Dawson TM, Dawson VL, Mediation of poly(ADP-ribose) polymerase-1-dependent cell death by apoptosis-inducing factor. Science 297, 259–263 (2002). [PubMed: 12114629]
38. Du L, Zhang X, Han YY, Burke NA, Kochanek PM, Watkins SC, Graham SH, Carcillo JA, Szabo C, Clark RS, Intra-mitochondrial poly(ADP-ribosylation) contributes to NAD+ depletion and cell death induced by oxidative stress. J Biol Chem 278, 18426–18433 (2003). [PubMed: 12626504]
39. Zong WX, Ditsworth D, Bauer DE, Wang ZQ, Thompson CB, Alkylating DNA damage stimulates a regulated form of necrotic cell death. Genes Dev 18, 1272–1282 (2004). [PubMed: 15145826]
40. Moubarak RS, Yuste VJ, Artus C, Bouharrour A, Greer PA, Menissier-de Murcia J, Susin SA, Sequential activation of poly(ADP-ribose) polymerase 1, calpains, and Bax is essential in apoptosis-inducing factor-mediated programmed necrosis. Mol Cell Biol 27, 4844–4862 (2007). [PubMed: 17470554]
41. Oka S, Ohno M, Tsuchimoto D, Sakumi K, Furuichi M, Nakabeppu Y, Two distinct pathways of cell death triggered by oxidative damage to nuclear and mitochondrial DNAs. EMBO J 27, 421–432 (2008). [PubMed: 18188152]
42. Ha HC, Snyder SH, Poly(ADP-ribose) polymerase is a mediator of necrotic cell death by ATP depletion. Proc Natl Acad Sci U S A 96, 13978–13982 (1999). [PubMed: 10570184]
43. Heeres JT, Hergenrother PJ, Poly(ADP-ribose) makes a date with death. Curr Opin Chem Biol 11, 644–653 (2007). [PubMed: 17936669]
44. Cipriani G, Rapizzi E, Vannacci A, Rizzuto R, Moroni F, Chiarugi A, Nuclear poly(ADP-ribose) polymerase-1 rapidly triggers mitochondrial dysfunction. J Biol Chem 280, 17227–17234 (2005). [PubMed: 15750180]
45. Alano CC, Garnier P, Ying W, Higashi Y, Kauppinen TM, Swanson RA, NAD+ depletion is necessary and sufficient for poly(ADP-ribose) polymerase-1-mediated neuronal death. J Neurosci 30, 2967–2978 (2010). [PubMed: 20181594]

46. Fouquerel E, Goellner EM, Yu Z, Gagne JP, Barbi de Moura M, Feinstein T, Wheeler D, Redpath P, Li J, Romero G, Migaud M, Van Houten B, Poirier GG, Sobol RW, ARTD1/PARP1 negatively regulates glycolysis by inhibiting hexokinase 1 independent of NAD+ depletion. Cell reports 8, 1819–1831 (2014). [PubMed: 25220464]
47. Wang Y, Kim NS, Haince JF, Kang HC, David KK, Andrabi SA, Poirier GG, Dawson VL, Dawson TM, Poly(ADP-ribose) (PAR) binding to apoptosis-inducing factor is critical for PAR polymerase-1-dependent cell death (parthanatos). Science signaling 4, ra20 (2011). [PubMed: 21467298]
48. Artus C, Boujrad H, Bouharrour A, Brunelle MN, Hoos S, Yuste VJ, Lenormand P, Rousselle JC, Namane A, England P, Lorenzo HK, Susin SA, AIF promotes chromatinolysis and caspase-independent programmed necrosis by interacting with histone H2AX. EMBO J 29, 1585–1599 (2010). [PubMed: 20360685]
49. Holler N, Zaru R, Micheau O, Thome M, Attinger A, Valitutti S, Bodmer JL, Schneider P, Seed B, Tschopp J, Fas triggers an alternative, caspase-8-independent cell death pathway using the kinase RIP as effector molecule. Nat Immunol 1, 489–495 (2000). [PubMed: 11101870]
50. Matsumura H, Shimizu Y, Ohsawa Y, Kawahara A, Uchiyama Y, Nagata S, Necrotic death pathway in Fas receptor signaling. J Cell Biol 151, 1247–1256 (2000). [PubMed: 11121439]
51. Vandenabeele P, Galluzzi L, Vanden Berghe T, Kroemer G, Molecular mechanisms of necroptosis: an ordered cellular explosion. Nat Rev Mol Cell Biol 11, 700–714 (2010). [PubMed: 20823910]
52. Degterev A, Huang Z, Boyce M, Li Y, Jagtap P, Mizushima N, Cuny GD, Mitchison TJ, Moskowitz MA, Yuan J, Chemical inhibitor of nonapoptotic cell death with therapeutic potential for ischemic brain injury. Nat Chem Biol 1, 112–119 (2005). [PubMed: 16408008]
53. Micheau O, Tschopp J, Induction of TNF receptor I-mediated apoptosis via two sequential signaling complexes. Cell 114, 181–190 (2003). [PubMed: 12887920]
54. Stanger BZ, Leder P, Lee TH, Kim E, Seed B, RIP: a novel protein containing a death domain that interacts with Fas/APO-1 (CD95) in yeast and causes cell death. Cell 81, 513–523 (1995). [PubMed: 7538908]
55. Cho YS, Challa S, Moquin D, Genga R, Ray TD, Guildford M, Chan FK, Phosphorylation-driven assembly of the RIP1-RIP3 complex regulates programmed necrosis and virus-induced inflammation. Cell 137, 1112–1123 (2009). [PubMed: 19524513]
56. He S, Wang L, Miao L, Wang T, Du F, Zhao L, Wang X, Receptor interacting protein kinase-3 determines cellular necrotic response to TNF-α. Cell 137, 1100–1111 (2009). [PubMed: 19524512]
57. Zhang DW, Shao J, Lin J, Zhang N, Lu BJ, Lin SC, Dong MQ, Han J, RIP3, an energy metabolism regulator that switches TNF-induced cell death from apoptosis to necrosis. Science 325, 332–336 (2009). [PubMed: 19498109]
58. Zhao J, Jitkaew S, Cai Z, Choksi S, Li Q, Luo J, Liu ZG, Mixed lineage kinase domain-like is a key receptor interacting protein 3 downstream component of TNF-induced necrosis. Proc Natl Acad Sci U S A 109, 5322–5327 (2012). [PubMed: 22421439]
59. Sun L, Wang H, Wang Z, He S, Chen S, Liao D, Wang L, Yan J, Liu W, Lei X, Wang X, Mixed lineage kinase domain-like protein mediates necrosis signaling downstream of RIP3 kinase. Cell 148, 213–227 (2012). [PubMed: 22265413]
60. Murphy JM, Czabotar PE, Hildebrand JM, Lucet IS, Zhang JG, Alvarez-Diaz S, Lewis R, Lalaoui N, Metcalf D, Webb AI, Young SN, Varghese LN, Tannahill GM, Hatchell EC, Majewski IJ, Okamoto T, Dobson RC, Hilton DJ, Babon JJ, Nicola NA, Strasser A, Silke J, Alexander WS, The pseudokinase MLKL mediates necroptosis via a molecular switch mechanism. Immunity 39, 443–453 (2013). [PubMed: 24012422]
61. Wang H, Sun L, Su L, Rizo J, Liu L, Wang LF, Wang FS, Wang X, Mixed lineage kinase domain-like protein MLKL causes necrotic membrane disruption upon phosphorylation by RIP3. Mol Cell 54, 133–146 (2014). [PubMed: 24703947]
62. Cai Z, Jitkaew S, Zhao J, Chiang HC, Choksi S, Liu J, Ward Y, Wu LG, Liu ZG, Plasma membrane translocation of trimerized MLKL protein is required for TNF-induced necroptosis. Nat Cell Biol 16, 55–65 (2014). [PubMed: 24316671]

63. Medzhitov R, Origin and physiological roles of inflammation. Nature 454, 428–435 (2008). [PubMed: 18650913]
64. Margulies CM, Chaim IA, Mazumder A, Criscione J, Samson LD, Alkylation induced cerebellar degeneration dependent on Aag and Parp1 does not occur via previously established cell death mechanisms. PLoS One 12, e0184619 (2017). [PubMed: 28886188]
65. Trichonas G, Murakami Y, Thanos A, Morizane Y, Kayama M, Debouck CM, Hisatomi T, Miller JW, Vavvas DG, Receptor interacting protein kinases mediate retinal detachment-induced photoreceptor necrosis and compensate for inhibition of apoptosis. Proc Natl Acad Sci U S A 107, 21695–21700 (2010). [PubMed: 21098270]
66. Murakami Y, Matsumoto H, Roh M, Suzuki J, Hisatomi T, Ikeda Y, Miller JW, Vavvas DG, Receptor interacting protein kinase mediates necrotic cone but not rod cell death in a mouse model of inherited degeneration. Proc Natl Acad Sci U S A 109, 14598–14603 (2012). [PubMed: 22908283]
67. Murakami Y, Matsumoto H, Roh M, Giani A, Kataoka K, Morizane Y, Kayama M, Thanos A, Nakatake S, Notomi S, Hisatomi T, Ikeda Y, Ishibashi T, Connor KM, Miller JW, Vavvas DG, Programmed necrosis, not apoptosis, is a key mediator of cell loss and DAMP-mediated inflammation in dsRNA-induced retinal degeneration. Cell Death Differ 21, 270–277 (2014). [PubMed: 23954861]
68. Baritaud M, Cabon L, Delavallee L, Galan-Malo P, Gilles ME, Brunelle-Navas MN, Susin SA, AIF-mediated caspase-independent necroptosis requires ATM and DNA-PK-induced histone H2AX Ser139 phosphorylation. Cell Death Dis 3, e390 (2012). [PubMed: 22972376]
69. Jang KH, Do YJ, Son D, Son E, Choi JS, Kim E, AIF-independent parthanatos in the pathogenesis of dry age-related macular degeneration. Cell Death Dis 8, e2526 (2017). [PubMed: 28055012]
70. Xu X, Chua CC, Zhang M, Geng D, Liu CF, Hamdy RC, Chua BH, The role of PARP activation in glutamate-induced necroptosis in HT-22 cells. Brain Res 1343, 206–212 (2010). [PubMed: 20451505]
71. Sosna J, Voigt S, Mathieu S, Lange A, Thon L, Davarnia P, Herdegen T, Linkermann A, Rittger A, Chan FK, Kabelitz D, Schutze S, Adam D, TNF-induced necroptosis and PARP-1-mediated necrosis represent distinct routes to programmed necrotic cell death. Cell Mol Life Sci 71, 331–348 (2014). [PubMed: 23760205]
72. Chen YY, Liu SL, Hu DP, Xing YQ, Shen Y, N -methyl- N -nitrosourea-induced retinal degeneration in mice. Experimental eye research 121, 102–113 (2014). [PubMed: 24509257]
73. Nambu H, Yuge K, Nakajima M, Shikata N, Takahashi K, Miki H, Uyama M, Tsubura A, Morphologic characteristics of N-methyl-N-nitrosourea-induced retinal degeneration in C57BL mice. Pathol Int 47, 377–383 (1997). [PubMed: 9211525]
74. Yuge K, Nambu H, Senzaki H, Nakao I, Miki H, Uyama M, Tsubura A, N-methyl-N-nitrosourea-induced photoreceptor apoptosis in the mouse retina. In Vivo 10, 483–488 (1996). [PubMed: 8899426]
75. Calvo JA, Allocca M, Fake KR, Muthupalani S, Corrigan JJ, Bronson RT, Samson LD, Parp1 protects against Aag-dependent alkylation-induced nephrotoxicity in a sex-dependent manner. Oncotarget, (2016).
76. Tinari A, Giammarioli AM, Manganelli V, Ciarlo L, Malorni W, Chapter one analyzing morphological and ultrastructural features in cell death. Methods Enzymol 442, 1–26 (2008). [PubMed: 18662562]
77. Burattini S, Falcieri E, Analysis of cell death by electron microscopy. Methods Mol Biol 1004, 77–89 (2013). [PubMed: 23733571]
78. Zhang H, Zhou X, McQuade T, Li J, Chan FK, Zhang J, Functional complementation between FADD and RIP1 in embryos and lymphocytes. Nature 471, 373–376 (2011). [PubMed: 21368761]
79. Kim YS, Morgan MJ, Choksi S, Liu ZG, TNF-induced activation of the Nox1 NADPH oxidase and its role in the induction of necrotic cell death. Mol Cell 26, 675–687 (2007). [PubMed: 17560373]
80. Sangiuliano B, Perez NM, Moreira DF, Belizario JE, Cell death-associated molecular-pattern molecules: inflammatory signaling and control. Mediators Inflamm 2014, 821043 (2014). [PubMed: 25140116]

81. Lotze MT, Tracey KJ, High-mobility group box 1 protein (HMGB1): nuclear weapon in the immune arsenal. Nat Rev Immunol 5, 331–342 (2005). [PubMed: 15803152]
82. Sims GP, Rowe DC, Rietdijk ST, Herbst R, Coyle AJ, HMGB1 and RAGE in inflammation and cancer. Annu Rev Immunol 28, 367–388 (2010). [PubMed: 20192808]
83. Bianchi ME, DAMPs, PAMPs and alarmins: All we need to know about danger. J Leukoc Biol 81, 1–5 (2007).
84. Ditsworth D, Zong WX, Thompson CB, Activation of poly(ADP)-ribose polymerase (PARP-1) induces release of the pro-inflammatory mediator HMGB1 from the nucleus. J Biol Chem 282, 17845–17854 (2007). [PubMed: 17430886]
85. Scaffidi P, Misteli T, Bianchi ME, Release of chromatin protein HMGB1 by necrotic cells triggers inflammation. Nature 418, 191–195 (2002). [PubMed: 12110890]
86. Linkermann A, Green DR, Necroptosis. N Engl J Med 370, 455–465 (2014). [PubMed: 24476434]
87. Krukenberg KA, Kim S, Tan ES, Maliga Z, Mitchison TJ, Extracellular poly(ADP-ribose) is a pro-inflammatory signal for macrophages. Chem Biol 22, 446–452 (2015). [PubMed: 25865309]
88. Vandenabeele P, Declercq W, Van Herreweghe F, Vanden Berghe T, The role of the kinases RIP1 and RIP3 in TNF-induced necrosis. Science signaling 3, re4 (2010). [PubMed: 20354226]
89. Los M, Mozoluk M, Ferrari D, Stepczynska A, Stroh C, Renz A, Herceg Z, Wang ZQ, Schulze-Osthoff K, Activation and caspase-mediated inhibition of PARP: a molecular switch between fibroblast necrosis and apoptosis in death receptor signaling. Mol Biol Cell 13, 978–988 (2002). [PubMed: 11907276]
90. Ba X, Garg NJ, Signaling mechanism of poly(ADP-ribose) polymerase-1 (PARP-1) in inflammatory diseases. Am J Pathol 178, 946–955 (2011). [PubMed: 21356345]
91. Daniels BP, Snyder AG, Olsen TM, Orozco S, Oguin TH 3rd, Tait SWG, Martinez J, Gale M Jr., Loo YM, Oberst A, RIPK3 Restricts Viral Pathogenesis via Cell Death-Independent Neuroinflammation. Cell 169, 301–313 e311 (2017). [PubMed: 28366204]
92. Gilley RP, Kaiser WJ, A RIPtide Protects Neurons from Infection. Cell Host Microbe 21, 415–416 (2017). [PubMed: 28407477]
93. Najjar M, Saleh D, Zelic M, Nogusa S, Shah S, Tai A, Finger JN, Polykratis A, Gough PJ, Bertin J, Whalen M, Pasparakis M, Balachandran S, Kelliher M, Poltorak A, Degterev A, RIPK1 and RIPK3 kinases promote cell-death-independent inflammation by Toll-like receptor 4. Immunity 45, 46–59 (2016). [PubMed: 27396959]
94. Newton K, Dugger DL, Maltzman A, Greve JM, Hedehus M, Martin-McNulty B, Carano RA, Cao TC, van Bruggen N, Bernstein L, Lee WP, Wu X, DeVoss J, Zhang J, Jeet S, Peng I, McKenzie BS, Roose-Girma M, Caplazi P, Diehl L, Webster JD, Vucic D, RIPK3 deficiency or catalytically inactive RIPK1 provides greater benefit than MLKL deficiency in mouse models of inflammation and tissue injury. Cell Death Differ 23, 1565–1576 (2016). [PubMed: 27177019]
95. Moriwaki K, Chan FK, Necroptosis-independent signaling by the RIP kinases in inflammation. Cell Mol Life Sci 73, 2325–2334 (2016). [PubMed: 27048814]
96. Vince JE, Wong WW, Gentle I, Lawlor KE, Allam R, O'Reilly L, Mason K, Gross O, Ma S, Guarda G, Anderton H, Castillo R, Hacker G, Silke J, Tschopp J, Inhibitor of apoptosis proteins limit RIP3 kinase-dependent interleukin-1 activation. Immunity 36, 215–227 (2012). [PubMed: 22365665]
97. Lawlor KE, Khan N, Mildenhall A, Gerlic M, Croker BA, D'Cruz AA, Hall C, Kaur Spall S, Anderton H, Masters SL, Rashidi M, Wicks IP, Alexander WS, Mitsuuchi Y, Benetatos CA, Condon SM, Wong WW, Silke J, Vaux DL, Vince JE, RIPK3 promotes cell death and NLRP3 inflammasome activation in the absence of MLKL. Nat Commun 6, 6282 (2015). [PubMed: 25693118]
98. Kang TB, Yang SH, Toth B, Kovalenko A, Wallach D, Caspase-8 blocks kinase RIPK3-mediated activation of the NLRP3 inflammasome. Immunity 38, 27–40 (2013). [PubMed: 23260196]
99. Du L, Bayir H, Lai Y, Zhang X, Kochanek PM, Watkins SC, Graham SH, Clark RS, Innate gender-based proclivity in response to cytotoxicity and programmed cell death pathway. J Biol Chem 279, 38563–38570 (2004). [PubMed: 15234982]
100. Hagberg H, Wilson MA, Matsushita H, Zhu C, Lange M, Gustavsson M, Poitras MF, Dawson TM, Dawson VL, Northington F, Johnston MV, PARP-1 gene disruption in mice preferentially

protects males from perinatal brain injury. J Neurochem 90, 1068–1075 (2004). [PubMed: 15312162]

101. McCullough LD, Zeng Z, Blizzard KK, Debchoudhury I, Hurn PD, Ischemic nitric oxide and poly (ADP-ribose) polymerase-1 in cerebral ischemia: male toxicity, female protection. J Cereb Blood Flow Metab 25, 502–512 (2005). [PubMed: 15689952]
102. Yuan M, Siegel C, Zeng Z, Li J, Liu F, McCullough LD, Sex differences in the response to activation of the poly (ADP-ribose) polymerase pathway after experimental stroke. Exp Neurol 217, 210–218 (2009). [PubMed: 19268668]
103. Liu F, Lang J, Li J, Benashski SE, Siegel M, Xu Y, McCullough LD, Sex differences in the response to poly(ADP-ribose) polymerase-1 deletion and caspase inhibition after stroke. Stroke 42, 1090–1096 (2011). [PubMed: 21311064]
104. Jog NR, Dinnall JA, Gallucci S, Madaio MP, Caricchio R, Poly(ADP-ribose) polymerase-1 regulates the progression of autoimmune nephritis in males by inducing necrotic cell death and modulating inflammation. J Immunol 182, 7297–7306 (2009). [PubMed: 19454727]
105. Jog NR, Caricchio R, Differential regulation of cell death programs in males and females by poly (ADP-ribose) Polymerase-1 and 17beta estradiol. Cell Death Dis 4, e758 (2013). [PubMed: 23928697]
106. Newton K, Sun X, Dixit VM, Kinase RIP3 is dispensable for normal NF-kappa Bs, signaling by the B-cell and T-cell receptors, tumor necrosis factor receptor 1, and Toll-like receptors 2 and 4. Mol Cell Biol 24, 1464–1469 (2004). [PubMed: 14749364]
107. Engelward BP, Weeda G, Wyatt MD, Broekhof JL, de Wit J, Donker I, Allan JM, Gold B, Hoeijmakers JH, Samson LD, Base excision repair deficient mice lacking the Aag alkyladenine DNA glycosylase. Proc Natl Acad Sci U S A 94, 13087–13092 (1997). [PubMed: 9371804]
108. Wang ZQ, Auer B, Stingl L, Berghammer H, Haidacher D, Schweiger M, Wagner EF, Mice lacking ADPRT and poly(ADP-ribosyl)ation develop normally but are susceptible to skin disease. Genes & Development 9, 509–520 (1995). [PubMed: 7698643]
109. Erickson PA, Fisher SK, Anderson DH, Stern WH, Borgula GA, Retinal detachment in the cat: The outer nuclear and outer plexiform layers. Invest Ophthalmol Vis Sci 24, 927–942 (1983). [PubMed: 6862796]
110. Hisatomi T, Sakamoto T, Goto Y, Yamanaka I, Oshima Y, Hata Y, Ishibashi T, Inomata H, Susin SA, Kroemer G, Critical role of photoreceptor apoptosis in functional damage after retinal detachment. Curr Eye Res 24, 161–172 (2002). [PubMed: 12221523]

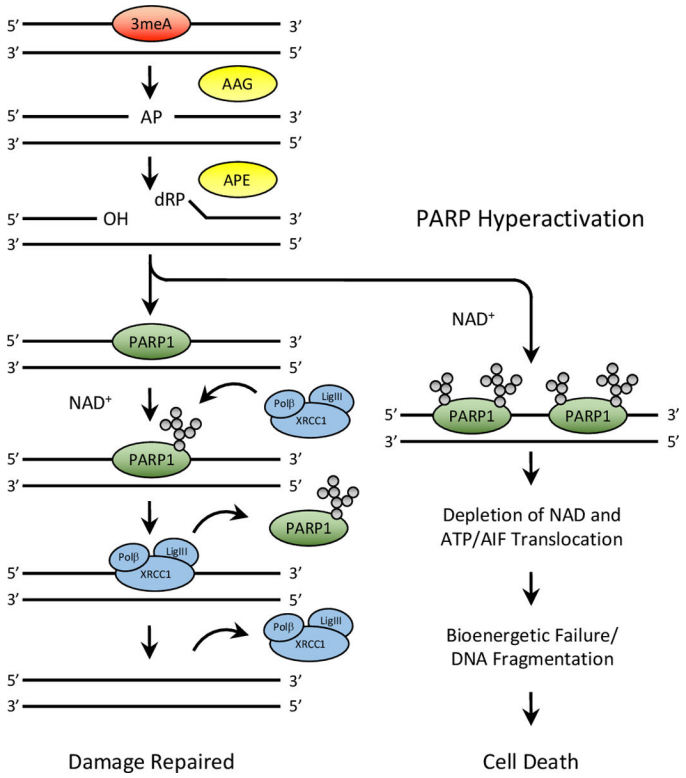

Fig. 1. Alkylation damage and the BER pathway.

AAG, alkyladenine DNA glycosylase; AP, apurinic/apyrimidinic site; OH, 3′OH terminus; XRCC1, x-ray repair cross-complementing protein 1; LigIII, ligase III; ATP, adenosine triphosphate; AIF, apoptosis-inducing factor.

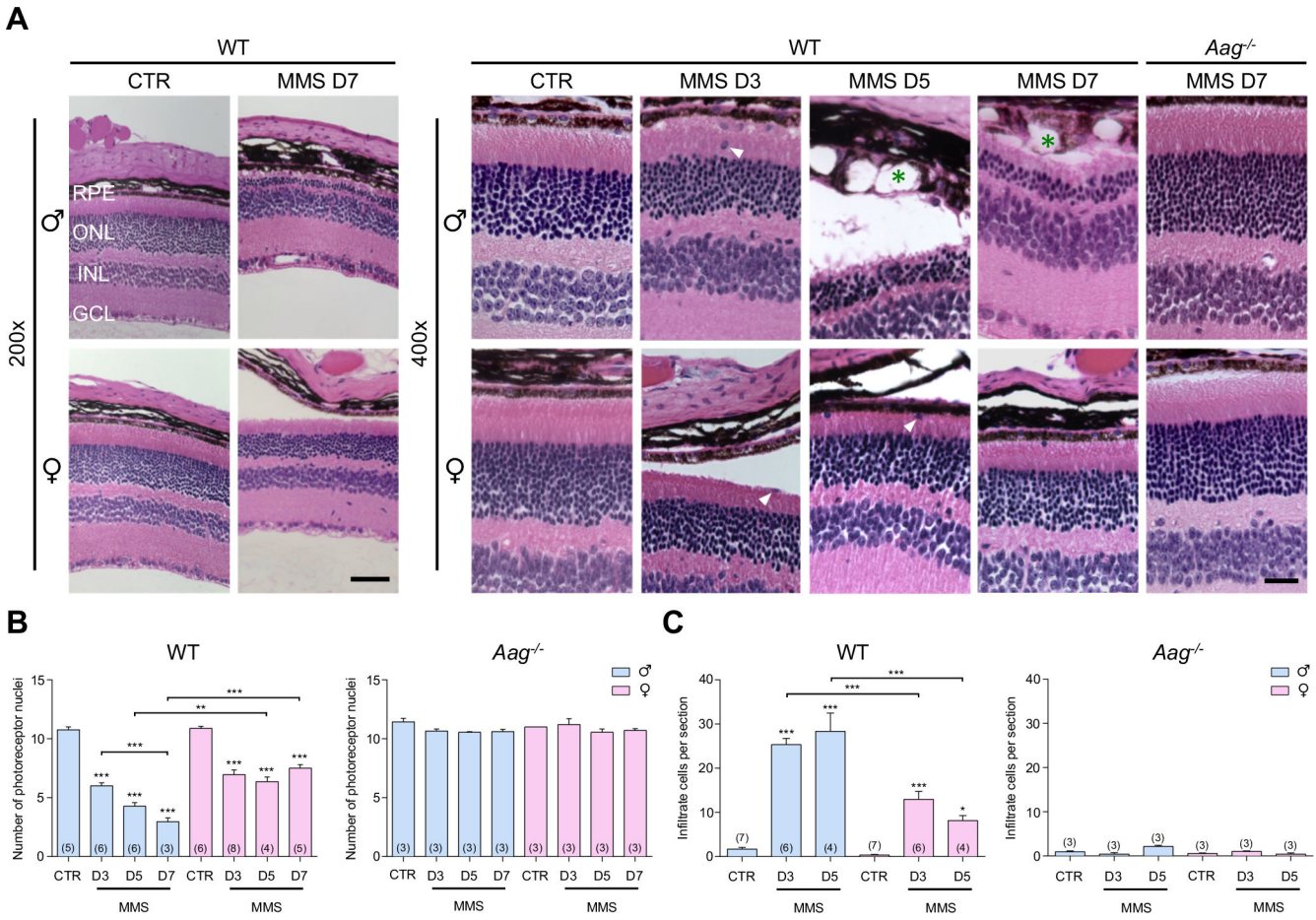

Fig. 2. MMS induces AAG- and sex-dependent PR degeneration, vacuolated RPE cells and subretinal cell infiltrates as early as 3 days after treatment.

(A) Representative hematoxylin and eosin (H&E)–stained images of retinas from WT and *Aag*$^{-/-}$ mice either untreated (CTR) or at 3, 5 and/or 7 days after injection with MMS (MMS D3, D5, and D7; 75 mg/kg). Scale bars, 50 μm (left, 200×) and 20 μm (right, 400×). INL, inner nuclear layer; GCL, ganglion cell layer; white arrowheads, cellular infiltrates; green asterisks, vacuolated and swollen RPE cells. **(B)** Quantification of rows of PR nuclei in the ONL of WT and *Aag*$^{-/-}$ mice at 3, 5, and/or 7 days after MMS treatment (75 mg/kg). **(C)** Number of subretinal cell infiltrates per section in WT and *Aag*$^{-/-}$ mice at 3 and 5 days after MMS (75 mg/kg). All data are means ± SEM; numbers of animals are indicated atop the bars (♂, males; ♀, females); *$P \leq 0.05$, **$P \leq 0.01$, and ***$P \leq 0.001$ by two-way analysis of variance (ANOVA) followed by Tukey's test.

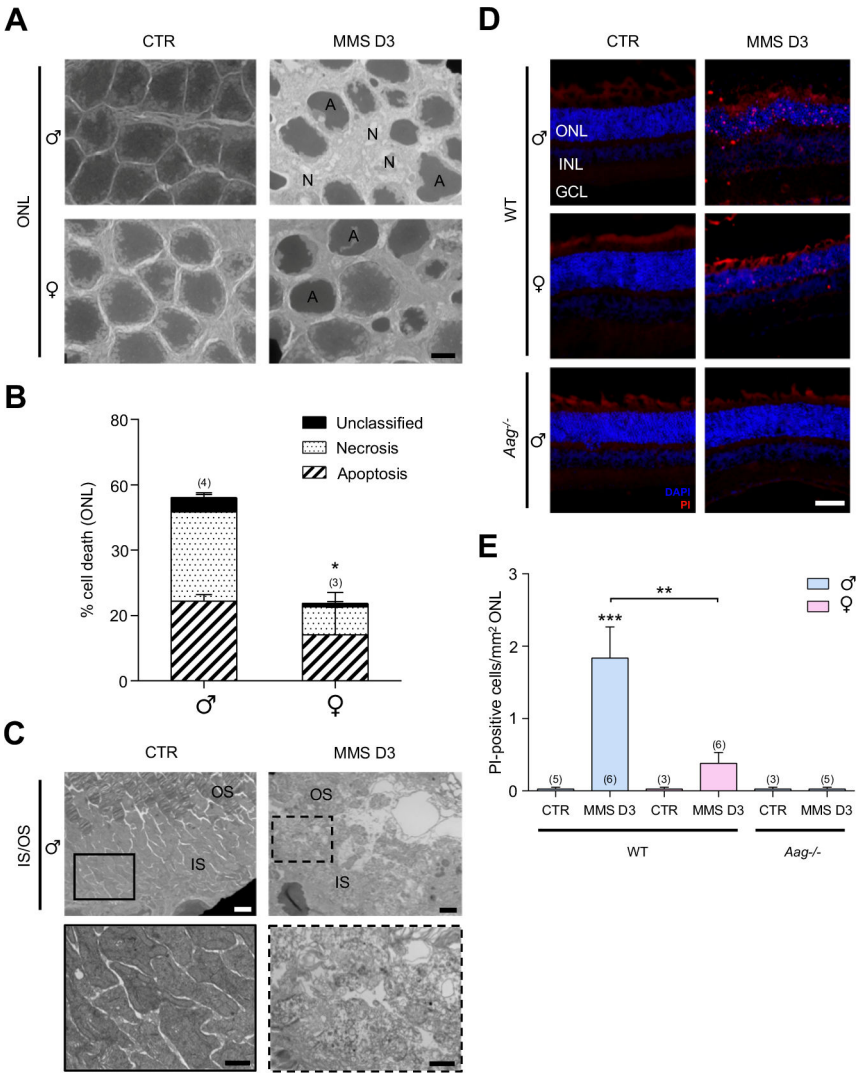

Fig. 3. MMS-induced PR cell death is associated with necrotic morphology.

(A) Electron microscopic photomicrographs of the ONL of WT male and female mice at day 3 after MMS (MMS D3; 75 mg/kg) injection; A, apoptotic nuclei; N, necroptotic nuclei. Scale bar, 2 μm. **(B)** Quantification of apoptotic and necrotic PR cell nuclei in the ONL of WT male and female mice at day 3 after MMS. **(C)** Electron microscopic photomicrographs of IS/OS of WT male mice at day 3 after MMS injection. Scale bars, 2 μm (top) and 800 nm (bottom). **(D and E)** Representative images of in vivo PI staining and quantification of PI-positive PRs in WT male and female mice and $Aag^{-/-}$ male mice on day 3 after MMS treatment (75 mg/kg). Scale bar, 50 μm. All data are means ± SEM; numbers of animals are indicated atop the bars; $*P \leq 0.05$, $**P \leq 0.01$, and $***P \leq 0.001$ by two-way ANOVA followed by Tukey's test. DAPI, 4′,6-diamidino-2-phenylindole.

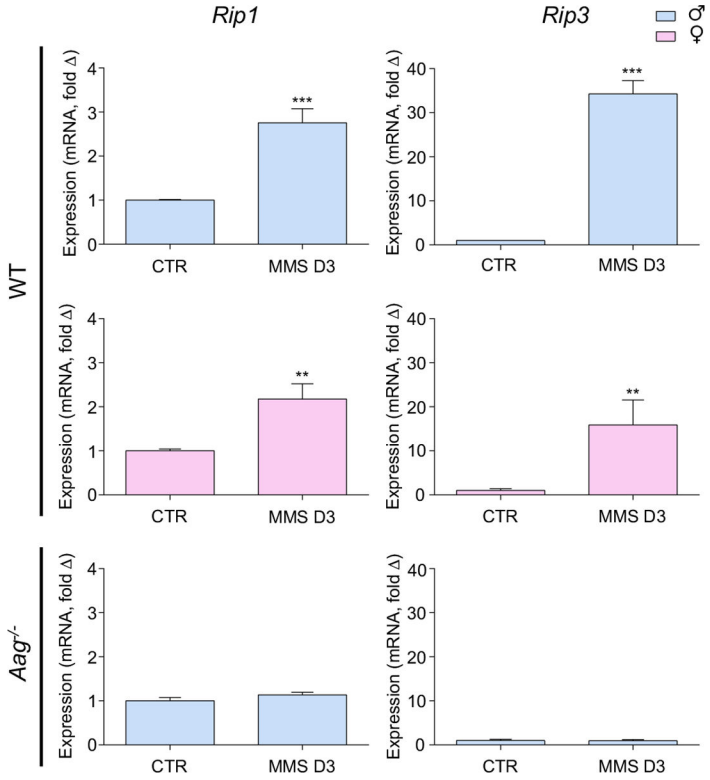

Fig. 4. MMS induces overexpression of *Rip1* and *Rip3* in the neuroretina of WT male mice.

Quantitative real-time PCR analysis for *Rip1* and *Rip3* expression in the neuroretina of WT male, WT female, and $Aag^{-/-}$ male mice at day 3 after MMS treatment (MMS D3; 75 mg/kg). Data are means ± SEM fold change (Δ) relative to untreated controls (CTR); n = 3 to 4 mice; $^{**}P \leq 0.01$ and $^{***}P \leq 0.001$ by unpaired *t* tests.

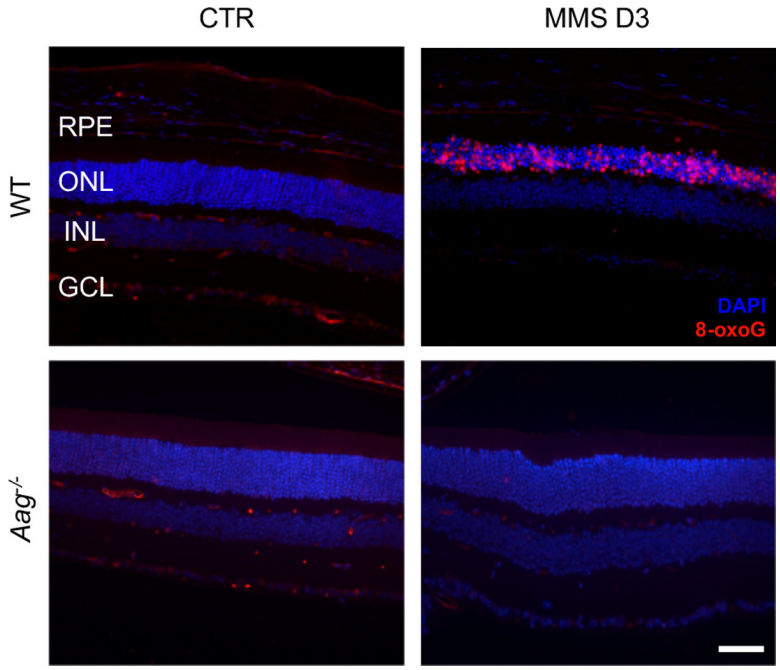

Fig. 5. MMS induces overproduction of ROS in PRs.

Representative immunofluorescence staining of 8-oxoG, an oxidative stress marker, in WT and *Aag*$^{-/-}$ male retina sections at day 3 after MMS treatment (75 mg/kg). Scale, bar 50 μm. Data are representative of n = 4 mice.

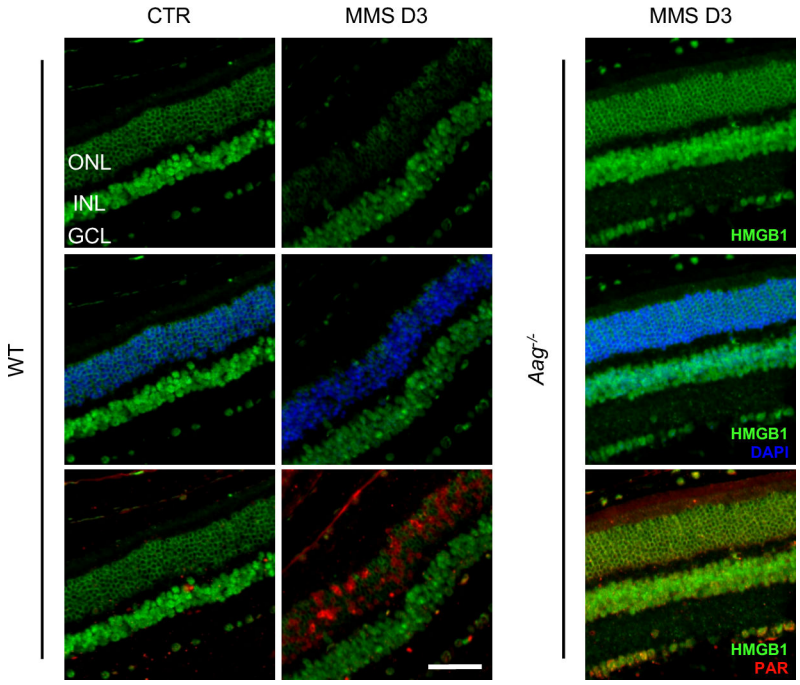

Fig. 6. MMS induces PARP activity in PR cells and the release of HMGB1 from PR nuclei.
Representative immunofluorescence images of PAR and/or HMGB1 on retinal sections from WT and *Aag*$^{-/-}$ male mice at day 3 after MMS treatment (MMS D3; 75 mg/kg). Scale bar, 50 μm. Data are representative of n = 3 mice.

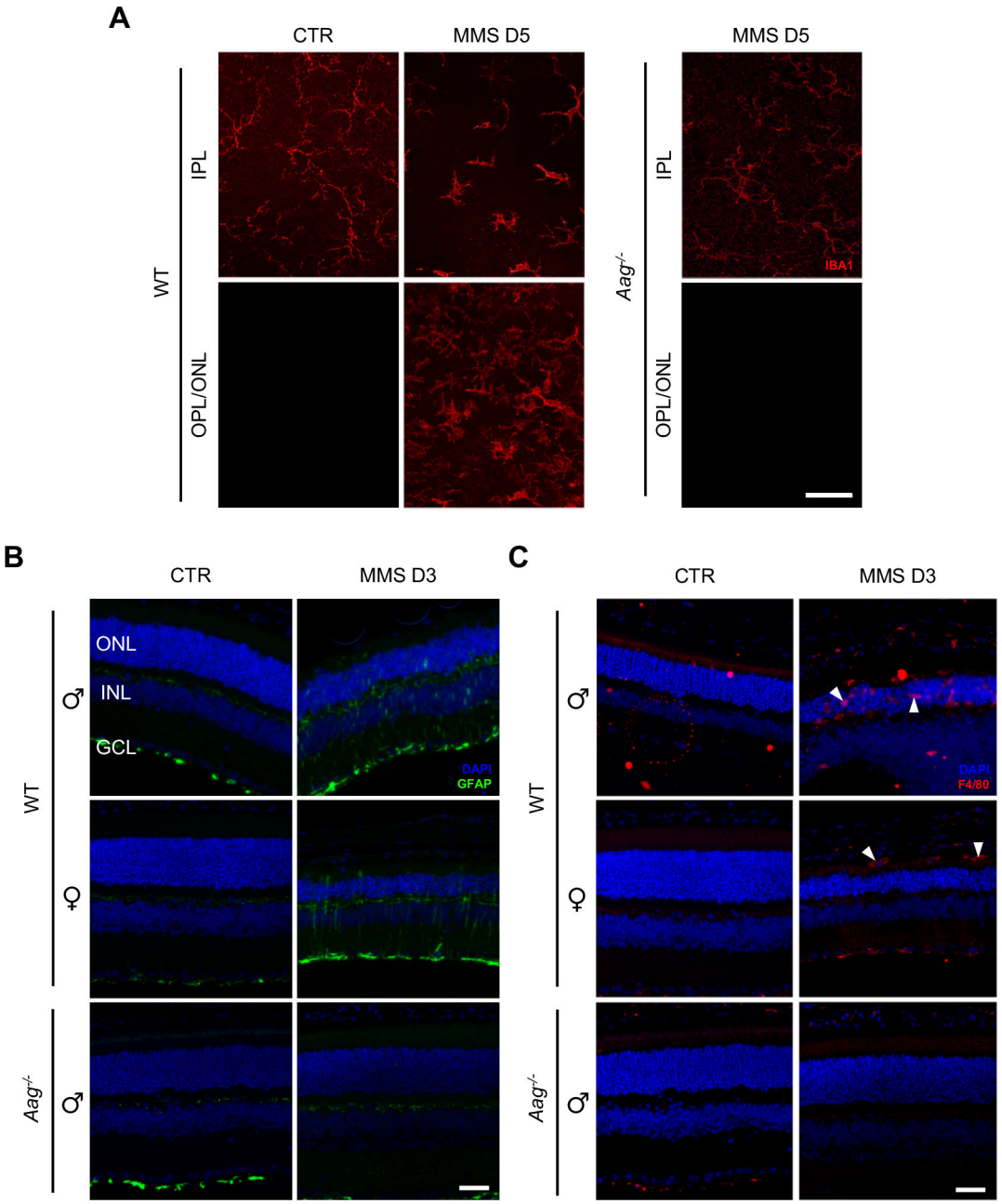

Fig. 7. MMS induces reactive gliosis and macrophage infiltration into the outer retina.

(A) Representative whole-mount immunofluorescence for IBA1 (microglial/macrophage marker) on WT and *Aag*$^{-/-}$ male retinas at day 5 after MMS treatment (MMS D5; 75 mg/kg). OPL, outer plexiform layer. Scale bar, 50 μm. **(B and C)** Representative immunofluorescence staining for GFAP (activated Müller glial marker; B) and for F4/80 (macrophage marker; C) on retinal sections from WT male and female and *Aag*$^{-/-}$ male mice at day 3 after MMS treatment (MMS D3; 75 mg/kg). White arrowheads, macrophages. Scale bars, 50 μm. Data are representative of n = 3 mice.

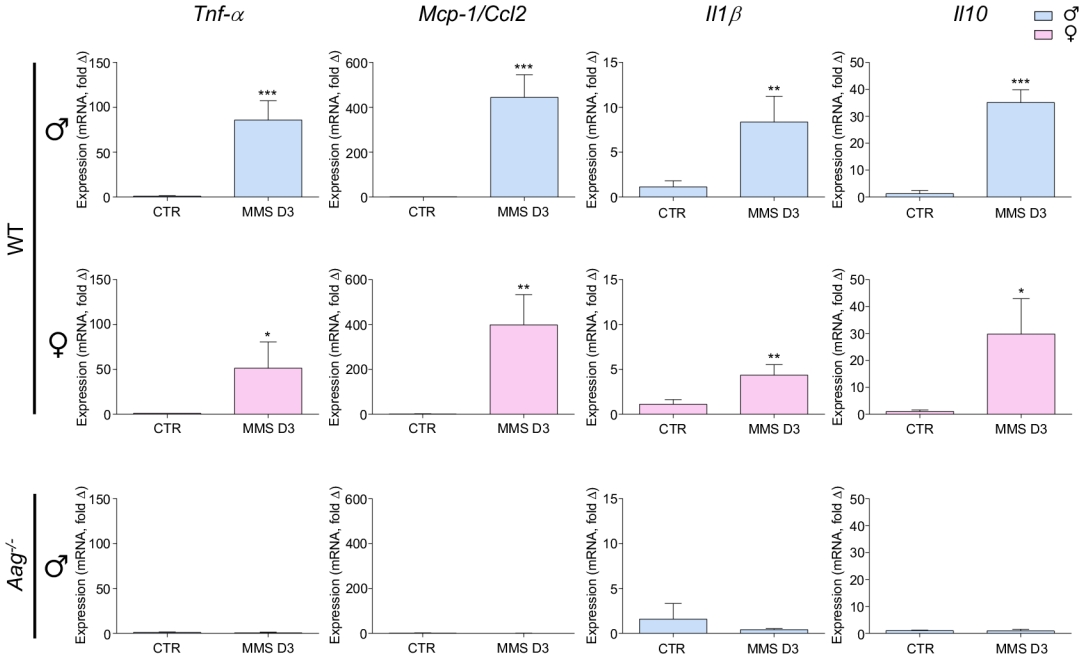

Fig. 8. MMS induces overexpression of inflammatory cytokines and chemokines in the neuroretina of WT male mice.

Quantitative real-time PCR analysis for proinflammatory markers *Tnf-α*, *Mcp-1* and *Il1*β and anti-inflammatory marker *Il10* in the neuroretinas of WT male, WT female, and $Aag^{-/-}$ male mice at day 3 after MMS treatment (MMS D3; 75 mg/kg). Data are means ± SEM fold change (Δ) relative to untreated controls (CTR); n = 3 to 5 mice; $*P \leq 0.05$, $**P \leq 0.01$, and $***P \leq 0.001$ by unpaired t tests.

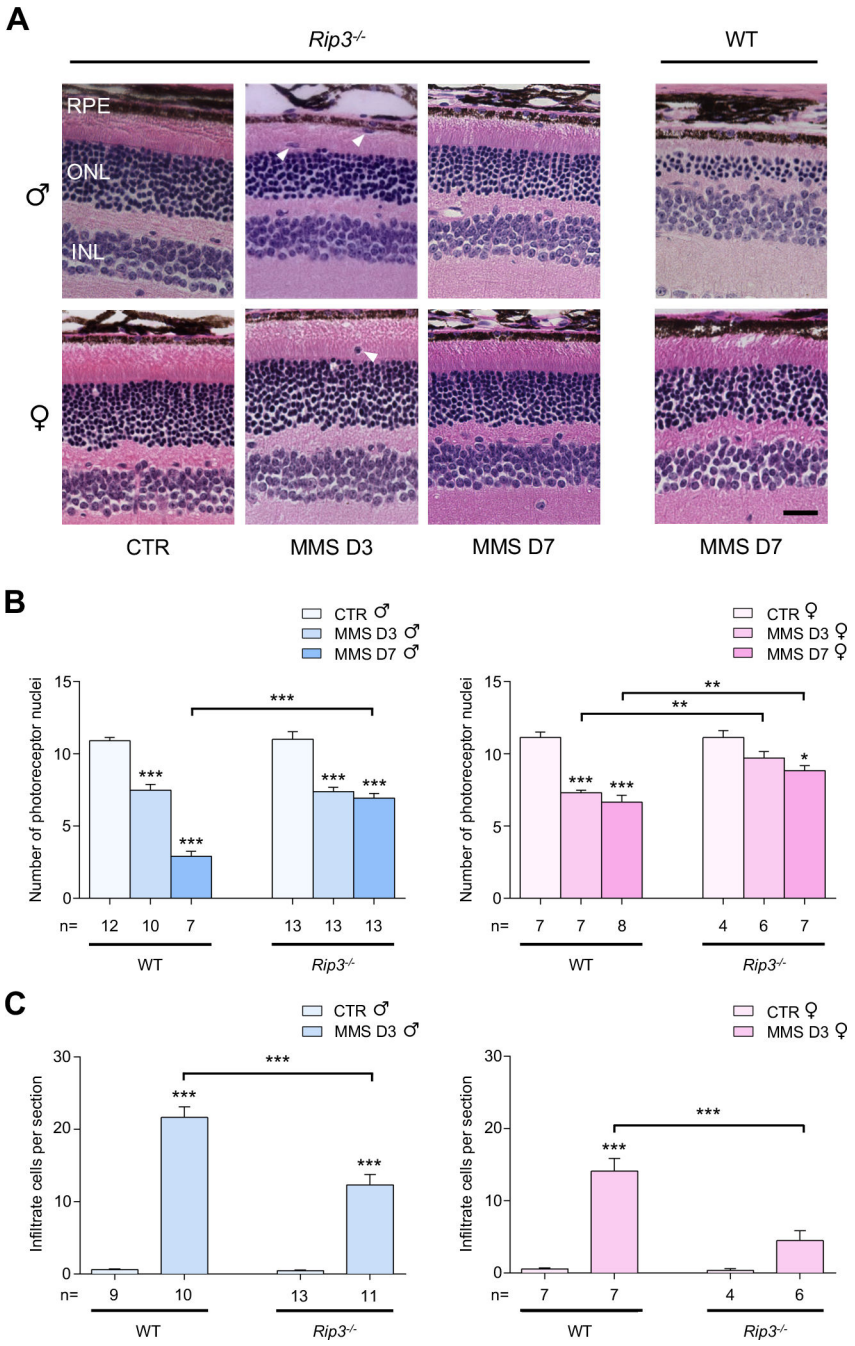

Fig. 9. RIP3 deficiency protects against MMS-induced RD and subretinal cell infiltration.

(A) Representative H&E-stained images of retinas from *Rip3*$^{-/-}$ and WT male and female mice either untreated (CTR) or at 3 and 7 days after MMS treatment (MMS D3 and D7; 75 mg/kg). Scale bar, 20 μm. **(B and C)** Number of rows of PR nuclei (B) in the ONL and number of subretinal cell infiltrates per section (C) in retinas from mice described in (A). Data are means ± SEM; numbers of animals (n) are indicated below the graphs; *$P \leq 0.05$, **$P \leq 0.01$, and ***$P \leq 0.001$ by two-way ANOVA followed by Tukey's test.

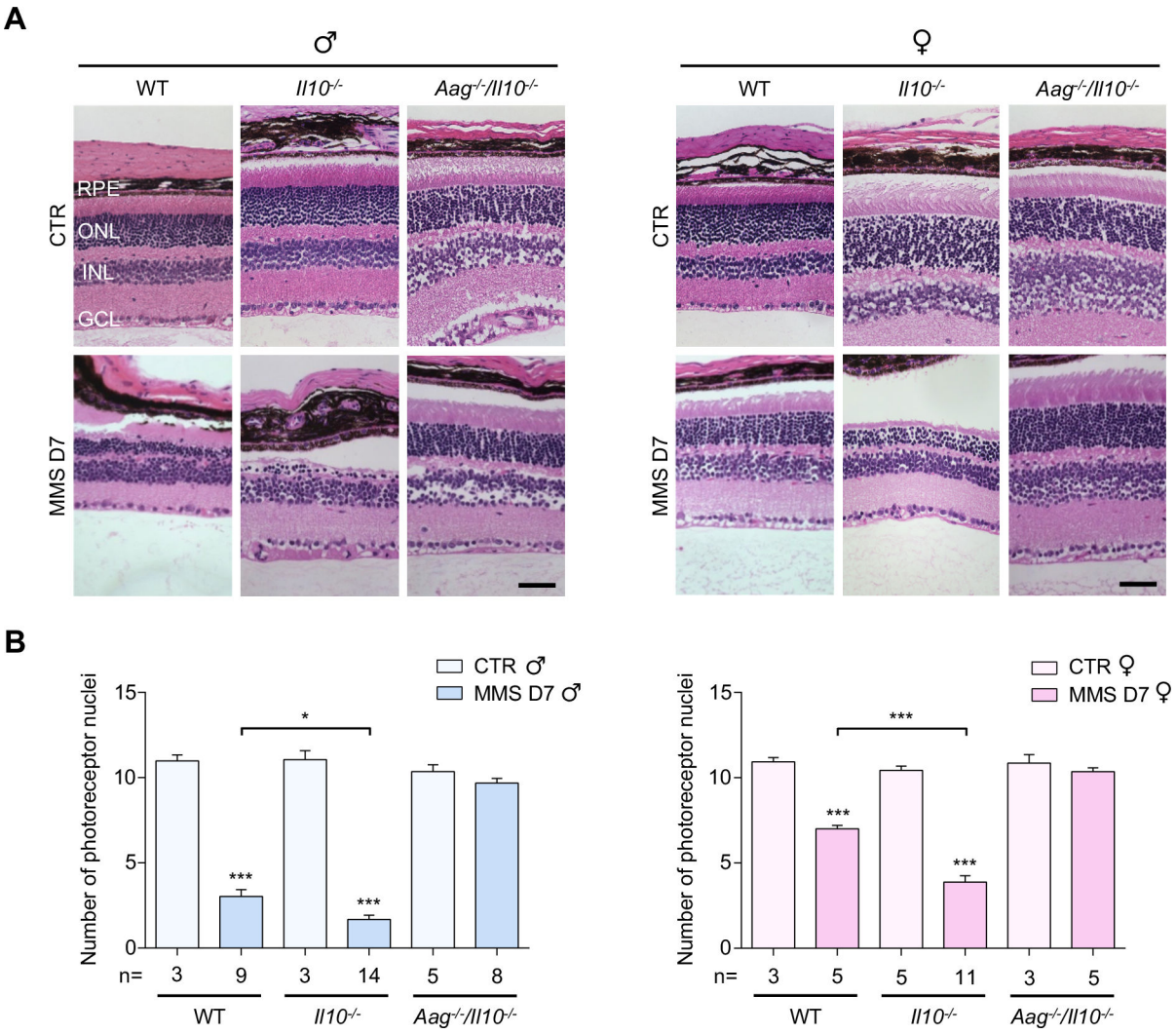

Fig. 10. Deficiency of IL-10 increases AAG-dependent, MMS-induced RD in both male and female mice.

(A and B) Representative H&E-stained images (A) and number of PR nuclei (B) in retinas from male and female WT, *Il10*$^{-/-}$, and *Aag*$^{-/-}$/*Il10*$^{-/-}$ mice either untreated (CTR) or at day 7 after MMS treatment (MMS D7; 75 mg/kg). Scale bars, 50 μm. Data are means ± SEM; numbers of animals (n) are indicated below the graphs; *$P \leq 0.05$ and ***$P \leq 0.001$ by two-way ANOVA followed by Tukey's test.

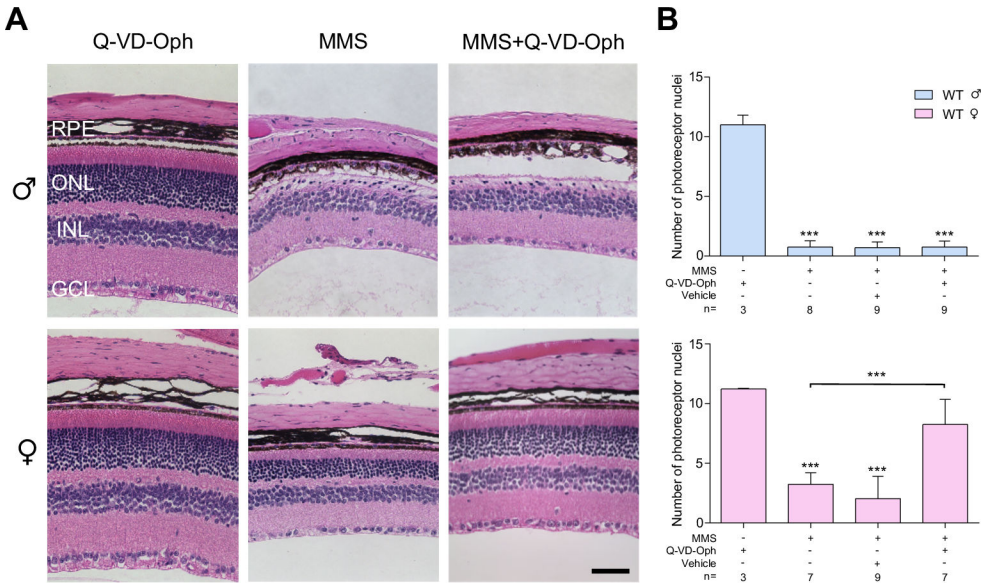

Fig. 11. Treatment with Q-VD-Oph, a pan-caspase inhibitor, protects WT female, but not male, mice from alkylation-induced RD.

(A and B) Representative H&E-stained images (A) and number of rows of PR nuclei (B) in the ONL of retinas from male and female WT mice either untreated (CTR) or at day 7 after MMS (MMS D7; 75 mg/kg) and/or Q-VD-Oph (10 mg/kg) treatment, as indicated. Scale bar, 50 μm. Data are means ± SEM; numbers of animals (n) are indicated below the graphs; ***$P \leq 0.001$ by one-way ANOVA followed by Tukey's test.